Modeling and simulation of a diesel engine cranking system.

Abstract

This master thesis is a study of the starting system for a diesel engine and its components. Theories for each component were presented and models were derived for a complete starting system. Focus lied on the starter motor and the losses in the diesel engine, and the models were implemented in the simulation environment Saber.

The starter motor model consists of a permanent magnet direct current (PMDC) motor with additional parts which complete the starter motor.

The loss components in the engine were manly derived from theoretical equations but also by measured data. The components were used as building blocks and put together to the entire engine losses model.

Measurements of the starting system were done and compared with the model's simulation results for different temperatures. The simulated average engine speed is approximately 20 % less than the measured.

Acknowledgement

First of all we would like thank our supervisors Johan Hellsing and Tomas Johannesson and our examiners Torbjörn Thiringer and Jonas Fredriksson. Thanks to Axel Nicklasson, Christer Andersson and André Jennert at Synopsys for help with the modelling and Saber. We would also thank Mikael Räim and Kjell Österlund for help with the measurements. Thanks to Bertil Andersson and all the other helpful people at the engine department at Volvo Cars for giving their knowledge about engines and its friction. Also many thanks go to the people at the Electrical department at Volvo Cars and to the component owners and suppliers, especially Javier Bores from Bosch, for providing us with useful data.

Contents

List Of Symbols

Symbol	Meaning	Unit
$T_e = T_{gen}$	generated torque in the strater motor.	Nm
Emf	generated voltage in the starter motor.	V
K_t	torque constant.	Nm/A
K_e	voltage constant.	V/rad/sec
T_{se}	number of armature turns per circuit.	
d	viscous damping coefficient	
ω_m	starter motor- rotor speed.	rpm
L_a	armature inductance.	H
R_a	armature resistance.	Ω
R_{br}	brush resistance.	Ω
R_{sll}	stray-load losses resistance in the starter motor.	Ω
$T_{q(rotor)}$	starter motor shaft-torque after the reduction gear.	Nm
P	starter motor output power.	
I_a	starter motor current.	A
U_{in}	starter motor input voltage.	V
U_{br}	brushes voltage-drop.	V
Sft	static friction losses.	W
U_k	battery-terminal voltage.	V
U_0	battery steady-state voltage.	V
U_l	no-load battery voltage.	V
R_i	battery-internal resistance.	Ω
R_c	cable power resistance	Ω
H	field strength.	A/m
B	flux density.	Tesla
ϕ	flux per pole.	Wb
f	frequency.	Hz
vol	volume of iron core.	m^3

K_h	proportionality constant from 1,5 to 2,5.	
K_e	proportionality constant from 1,5 to 2,5.	
B_m	maximum value of flux density.	Tesla
τ	lamination thickness.	m.m

Chapter 1

Introduction

1.1 Background

Computer simulations which accurately simulate complex physical systems have become valuable tools in many applications, such as design, analysis and development of control algorithms.

Simulation of the automotive engine cranking system can be based on theoretical models of the behaviour of the engine, the battery and the starter motor, respectively, during cranking. Modelling and simulating the dynamic operation of cranking systems is necessary in order to enable an “a priori” selection of the correct design parameters. This requires a good understanding of the various dynamic phenomena occurring during the cranking operation and development of accurate dynamic models for system simulation. Without such tools, the designer is left to cut-and-try empirical design approach, which might requires costly redesigns before a satisfactory operation of the cranking system is achieved.

1.2 Objective

The objective of this Master of Science thesis is to simulate the starting system of a diesel engine during cranking by creating proper models for the diesel engine and the starter motor. The model should be implemented and simulated using the simulation software Saber and should be valid within the temperature span of - 30°C to + 90°C.

The thesis includes performing measurements of the cranking operation in a real starting system for different temperatures between - 30°C and + 90°C. The starting model should be compared with the results from the empirical data. The model will, in the future, after further improvement be used to obtain the

characteristics of the starter motor and the engine during cranking, especially in cold temperatures, at Volvo Cars.

1.3 Methodology

The main methodology is to derive models of the starting system and thereby gain knowledge. The work started with studies of existing literature and papers about modelling starting systems and followed by education in the chosen simulation software. The model parts are implemented in Saber and its description language Mast. In addition to the simulations, measurements of the cranking in Volvo's diesel engine called NED were performed. Finally, the measurements and simulations results were compared.

1.4 Thesis overview

This first chapter gives the background and presents the goals of the thesis. The chosen simulation environment is described in the Saber overview. Chapter 2, 3, 4 and 5 introduces different parts of the starting system and begin with introduction and basic theory of the component followed by the corresponding model. Thereafter, in Chapter 6 the results from the practical measurements are described. In Chapter 7, the results from the simulations are shown. Finally, in Chapter 8, the conclusions of the thesis are discussed.

1.5 Overview of the simulation software

The simulations were performed using the program Saber[1]. This software is used to simulate physical effects in different engineering domains (hydraulic, electric, electronic, mechanical, etc.) as well as signal-flow algorithms and software. The Saber software is used in the automotive, aerospace, power and industries to simulate and analyze systems, sub-systems and components to reduce the need for prototypes. The largest model library in the industry, advanced analyses, integration in popular design environments and support for standard hardware description languages such as MAST and VHDL-AMS help engineers to create more robust and cost efficient designs faster [1].

[1] Saber is a registered trademark of Synopsys, CA, USA

Saber uses modified nodal analysis (MNA) to formulate its equations. This is similar to the nodal analysis of electrical circuits. There is at least one across variable and one through variable for each input- output of a component.

The MAST Hardware Description Language (HDL) from Synopsys is the de facto industry standard. First released in 1986, MAST is the most advanced modelling language available for analog, mixed-signal and mixed-technology applications. [2]

Chapter 2

Battery and Cable

2.1 Introduction

The vehicle battery is used as a source of energy in the vehicle when the engine, and hence the alternator, is not running. It must fulfill many requirements in a wide temperatures range.

2.2 Theory

2.2.1 Battery

The battery is not in focus in this thesis work since it is complicate and needed deep studying and searching to be able to model it.

In fact the starter motor generally obtains its electrical power supply from a lead-acid accumulator battery (Where a 12 V battery has six cells connected in series). The available voltage / current in cold weather are lower because the internal impedance of this type of battery increases as the temperature decrease.

The most important battery characteristic as far as starting the engine is concerned is it's power capability, which is the product of the supplied current (I) and the voltage between the terminals (U_k).

The internal resistance (R_i) of the starter battery has a diminishing effect on the starter motor power output in addition to the resistance of the power cable, switches and contacts. However, the internal resistance of the battery is not a fixed quantity, it is a variable which is dependent not only on the battery design but also the temperature (were the internal resistance R_i proportional

inversely with the temperature), the battery charge level, battery age, and usage history.

Figure 2.1 shows a simplified battery characteristic graph, when the battery is fully charged, the voltage drops steeply at low level of the current draw. At a higher level of current draw, the gradient of the graph is shallower, this is the range in witch the battery is operating during the starting sequence.

therefore, It makes sense to define the internal resistance of the battery for the starting within this range. All the processes for determine the internal resistance (R_i) can be found in [1], Further studies for the battery characteristics can be found in [2].

Thus, the internal resistance (*Ri*) is given by

$$R_i = (U_0 - U_f) / I_{cc} \tag{2.1}$$

and the simplified battery characteristic is given by

$$U_k = U_0 - R_i I \tag{2.2}$$

where U_k is the battery-terminal voltage, and that shown clear in figure 2.2.

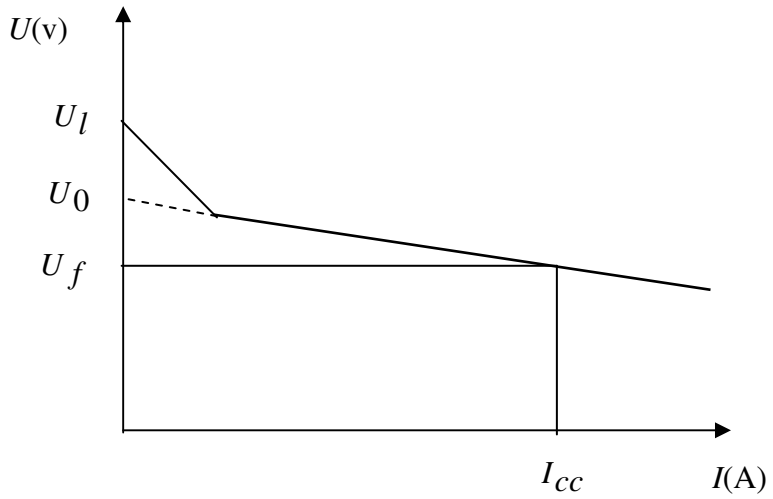

Figure 2.1: Steady-state relation between current and voltages for a fully charged battery.

I_{cc} low-temperature test current, U_f voltage at low-temperature test current U_0 steady- state voltage, U_l no-load voltage.

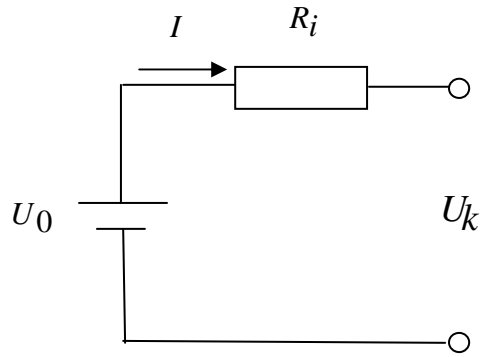

Figure 2.2: The simplified battery circuit.

2.2.2 Cable

The power-supply cable to the starter motor has a fundamental effect on the power of the starting system. Under normal conditions, it has to carry the starter-motor short-circuit current for a short period, and the current required to turn the engine over for the duration of the starting sequence.

For that; cable with a big dimension are used to ensure that the high currents can be handled while keeping the voltage drop as low as possible, which of course should not be above the permissible level (voltage drop) between the battery and the starter.

The cable resistance R_C is proportional to the length l and inversely with Cross-section A as seen in the Equation(2.3):

$$R_C = \frac{\rho l}{A} \tag{2.3}$$

Where ρ is the material resistivity.

On the other hand the length of the cable should be considered to ensure a low voltage drop.

2.3 The model

2.3.1 Battery

A simple model was used for the battery which is a constant voltage source connected in series with the internal resistance R_i .

The voltage value and the corresponding R_i at specific temperature were obtain from the characteristics those supplied by Bosch.

2.3.2 Power cable

The power cable modeled as a temperature dependent resistance, by that lower resistance at lower temperature and that represented by the following relation:

$$r(t) = r_{nom}(1 + \alpha(t - t_{nom})) \quad (2.4)$$

Where *r (t)* is the resistance at desired temperature, r_{nom} is the resistance at $t = 27$ °C, *t* is the climate temperature, t_{nom} is equal to 27 °C, and α is armature winding resistance temperature coefficient where the default value is 0,0039 for Copper material.

Chapter 3

Starter Motor

3.1 Overview

The starter motor is an electric DC motor that is used for starting engine. In other words the starter motor mission is to convert the electrical energy that stored in the battery to a mechanical energy that gives the combustion engine the initial speed until it will be able to run by itself.

In this chapter the starter motor is in focus. It starts with DC motor design and principle continues with PMdc motor's features and characteristics, the main components in the starter motor; planetary gear, solenoid and overrun clutch and the starter motor operation. Finally the starter motor is modeled and a suggestion for future work will end this chapter.

The interested radar can find more details about the starter motor in [3], [4] and [5] .

3.2 Introduction

The study and simulation model for the starter motor in this thesis will be on the starter motor type Bosch R78-M45, this type of starter motors is a PMdc motor with complementary components which complete the starter motor.

3.3 DC Motor

3.3.1 DC motor design

In the DC motor the stationary part of the motor is called the stator where the stator field is created either by permanent magnets, or by the use of a field coil.

The moving part of the motor is called the rotor or armature; it consists essentially of the laminated core that is press-fitted onto the armature shaft and

serves to conduct magnetic flux. On its outer circumference the laminated core has slots into which copper wires are inserted or laid, the wires are connected to each other according to a specific winding pattern and welded to the plates of the commutator, collectively they form the armature winding.

The current that flows through the armature winding is supplied through carbon brushes, these are in sliding contact with the commutator and thus distribute the current in sequence to the individual plates of the commutator as it rotates.

These brushes are often made of a mixture of copper and carbon; they have a higher copper content to minimize the electric losses.

3.3.2 The principle of operation of DC motor

Since the flow of the electric current through conductors in a magnetic field produces a force in accordance with Biot-Savarts Law $F = BLI$ (where B is the magnetic flux density, L is the length of the conductor, I is the current flowing in the conductor, F is the force, the effect of commutation is to create a torque, Te represented by the equation: $T_e = Fr$, where r is the radius of the rotor. That finally leading to:

$$T_e = T_{gen} = K_t I \tag{3.1}$$

where Kt is the torque constant and it is expressed as

$$K_t = \frac{p}{\pi} \Phi T_{se} \tag{3.2}$$

Where K_t is the torque constant (Nm /A), p is the number of the poles, Φ is the flux per pole, T_{se} is the number of armature turns per circuit (i.e. turns that are connected in series).

Furthermore voltage is induced in wire coil that is moving inside a magnetic field in accordance with the Faraday's Law $E = BLv$, B and L are the same as

before, v is the motional speed of the conductor (armature) with respect to the magnetic field.

The generated voltage ($Emf = E$) is represented by the equations $v = r\omega_m$ and by constitute in $E = BLv$ that as result leads to

$$E = Emf = K_e \omega_m \qquad (3.3)$$

This voltage appears externally as DC voltage. Ke is the voltage constant (V/ rad/ sec), ω_m is the angular speed of the rotor.

($K_e = K_t$ numerically) if the selected units system is SI.

$$K_e = K_t = \frac{p}{\pi} \Phi T_{se} \qquad (3.4)$$

3.4 The permanent magnet motor (PMdc motor)

In this type of dc motor the stator field is created by permanent magnet material which is usually mounted on the stator,

The PMdc motor is nowadays widely used in the starting system of the automotive cars due to it's advantages compared with the other types of the starters motor.

3.4.1 Permanent magnetic material

The permanent magnetic materials are hard magnetic materials characterized by large hysteresis loops, like Ceramic Ferrites, Alnico and other materials.

The hysteresis loops is determine by Hc, Br. as shown in Figure 3.1

- H_c (coercivities): the value of magnetizing field at which the flux density in the magnet reaches zero. The value of H_c is considerably high in the hard magnetic material (HMM) comparable to the soft magnetic material (SMM) at least 1KA/M for (HMM) while it is few

A/M for the (SMM) in some applications. The magnitude of coercivities indicates the material's magnetic hardness.

- B_r (remanence or residual flux): the value flux density when the field strength is zero.

Now we can define the maximum energy product (*BH*) max as it represent the maximum energy available from the magnet and it is equal to the product of B_r and H_c. The higher value of (*BH*) max that the material has the smaller volume of magnet material is required to produce a given magnet flux.

The main reason for using Ceramic Ferrites instead of other magnet materials, is that the Ferrites have a positive temperature coefficient, that means: the remanence (B_r) of Ferrites will increase when the temperature decrease and that will play an important roll during cranking at low temperature, while most of the other magnetic materials have a negative temperature coefficient.

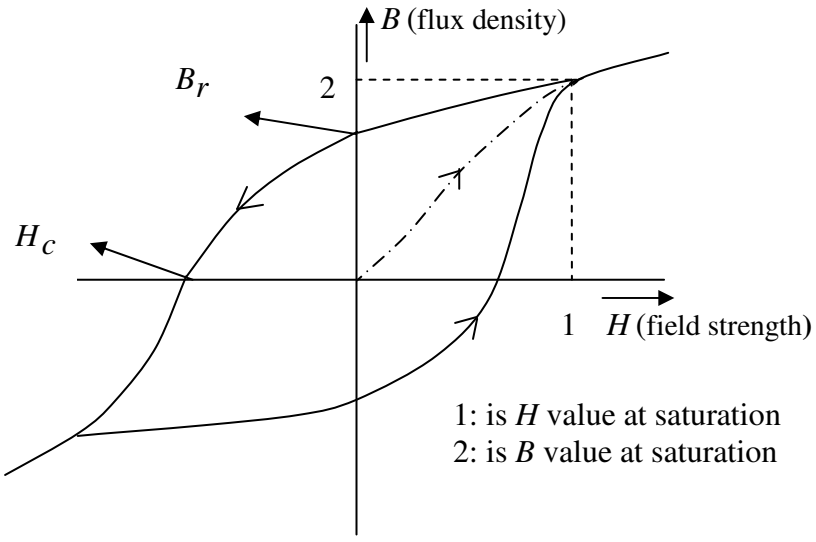

Figure 3.1: B-H loop of a hard magnetic material.

3.4.2 The advantages and characteristic of (PMdc motor)

The main advantages of these motors compared with wound field motors are:

1- Less weight (in the region of 15%). [4]

2- Smaller size.

Nowadays these advantages are considerably important since they provide more space and less weight in the vehicle.

The PMdc motors provide constant excitation (for constant temperature) i.e. the excitation is independent of the armature current, which means the torque will increases linearly with the current, while the motor speed decrease linearly with the current, and the output power characteristic is represented by a convex (parabolic curve).

In Figure 3.2 the relationships between torque, speed, out put power versus current are shown.

Real start motor characteristics are marginally different from the theoretical graphs that is due in particular to the retroactive effect of the armature magnetic–field at high current, but also because of other factors such as nonlinear material and friction.

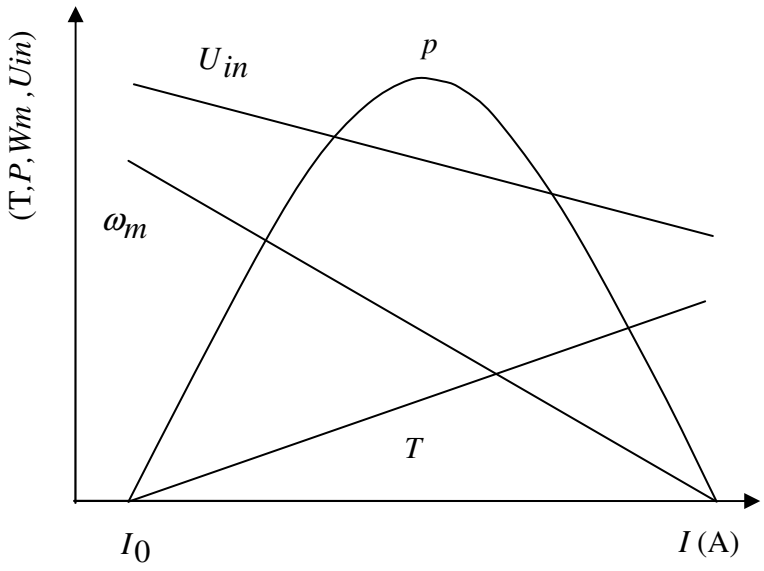

Figure 3.2: Characteristics of PMdc.

Where T is the torque in Nm, P is the power in kw, ω_m is the speed in rpm, U_{in} is the starter input voltage in V and I_0 is the no-load current.

3.4.3 PM motor with flux concentration

The aim of this process is to change the torque and speed characteristic of the PM motor to get close to the series-wound characteristic (where the relations between the torque–speed versus current are not any more linearly) so as a result the torque and the no-load speed will increase.

In this process, part of the leading edge of the magnet is replaced by a piece of soft iron as it shown in figure 3.3. As the size of the magnet is smaller and the soft-iron piece short-circuits part of the magnet flux, the primary flux is reduced under no-load conditions, and that lead to increase the no-load speed.

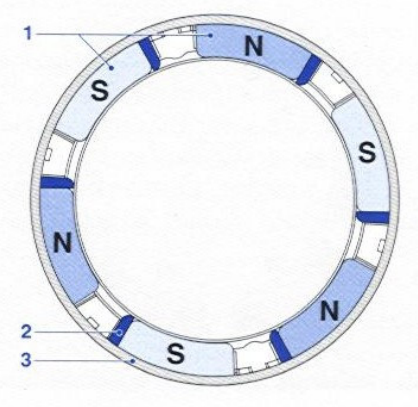

1- Permanent magnet.
2-Flux concentration .
3-Stator housing.

Figure 3.3: Stator housing with permanent magnet and flux concentration.

In the vicinity of the short-circuit, the soft-iron pole edge offer a path of high magnetic conductivity for the flux resulting from the stator flux and the armature flux, and as a result the overall flux is greater and the torque is higher under load condition compared with the motors without flux concentration.

- Flux concentrators are primarily a common feature of medium-power starter motors for car diesel engines.

Figure 3.4 illustrate the effect the flux concentration compared to the Figure 3.2.

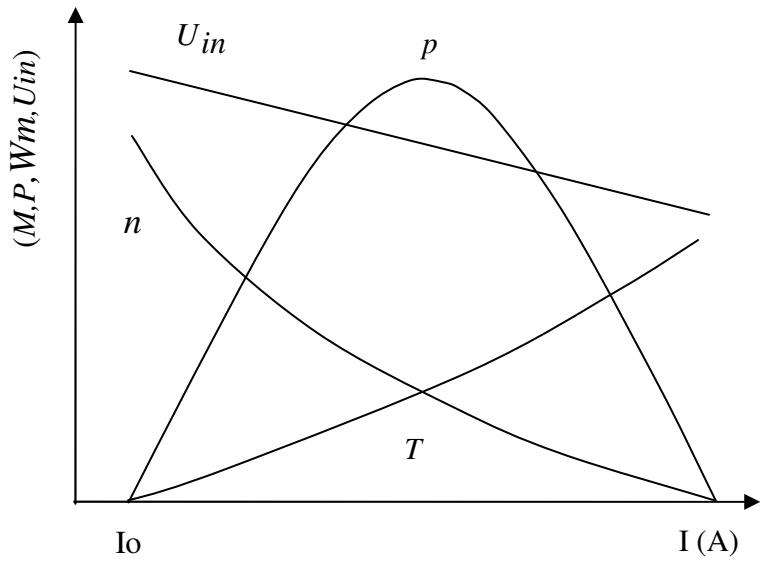

Figure 3.4: Characteristics of (PMdc motor) with flux concentration.

3.5 The used starter motor

3.5.1 Main circuit

The electric circuit of the starter motor is shown in Figure 3.5. The voltage at the battery terminals U_k, is the result of the open- circuit voltage U_l minus the voltage drop due to the battery's internal resistance R_i.

The voltage available at the starter motor, U_{in} is further reduced by the voltage drop due to the power cable resistance R_c. The voltage at the commutator is in turn diminished by the voltage drop due to the brushes U_{br}. Approximately 1.2 V is generally lost for each pair of the brushes, for positive and negative combined, therefore $U_{br} \approx 2.4$ V. The resistance of the armature in the starter motor is R_a.

For this electric circuit and based on the Kirchhoff's Law and the Equations (3.1) and (3.3) in the section 3.3.2 we can write:

$$U_l = (R_i + R_c + R_a)I + U_{br} + Emf \quad (3.5)$$

$$U_l = (R_i + R_c + R_a)I_+ U_{br} + K_e\omega_m \quad (3.6)$$

$$\omega_m = (U_l - (R_i + R_c + R_a)I - U_{br})/K_e \quad (3.7)$$

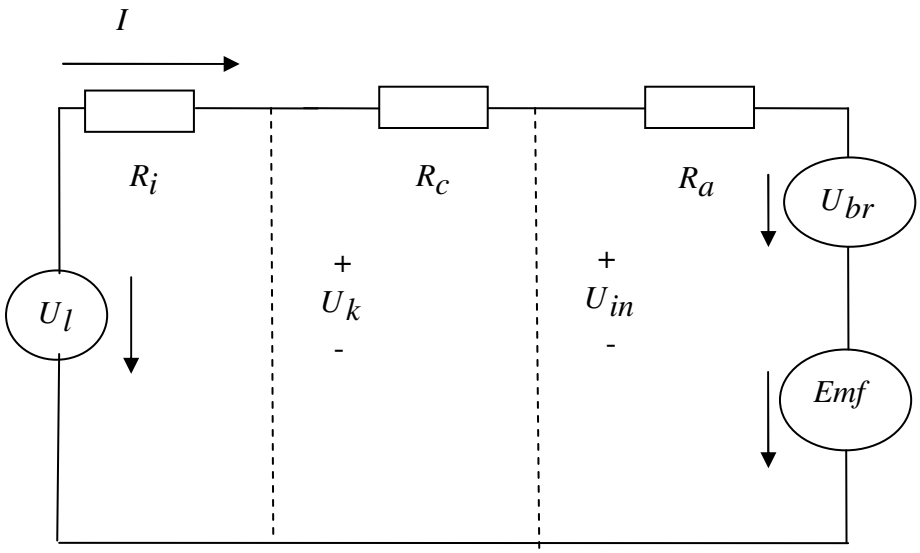

U_l: open-circuit battery's voltage.
U_k: voltage at the battery terminals.
U_{in}: voltage at the starter motor terminals.
U_{br}: brushes voltage drop.
Emf: generated voltage.
R_i: internal battery's resistance.
R_c: cable resistance.
R_a: armature resistance.

Figure 3.5: Starter-motor main circuit.

3.5.2 Operation of the starter motor

When the starter switch is operated, the battery voltage is applied to the terminal 50 in the solenoid, this causes two windings to be energized, the Hold-in winding and the pull-in winding. The magnetic force pulls in the solenoid plunger against the force of the plunger return spring, causing the shift lever to push the clutch drives assembly toward the ring gear, as it is seen in figure 3.6.

Depending on the relative angular position of the pinion and ring gear teeth, the pinion will either engage directly with the ring gear or abut it.

In the case of the direct engagement, and when the pinion at the end of its travel is fully in mesh with the ring gear, a set of copper contact is closed at the same time. These contacts now supply full battery power to the main circuit of the starter motor.[4]

When the main contacts are closed, the pull-in winding is effectively switched off due to equal voltage supply on both ends. The Hold-in winding holds the plunger in position as long as the solenoid is supplied from the starter switch, by that the motor transmits the torque to the clutch drive, which in turn transmits the torque to the pinion through the overrunning clutch.

As a result when the starter motor begins to rotate, the transmission ratio between the pinion and the ring gear produces a large amount of torque acting on the crankshaft of the engine, the frictional resistance is over come and the engine start to turn over.

When the engine starts and the key is released, the main supply is removed and the plunger and the pinion return to their rest positions.

In the case of a pinion to ring-gear tooth abutment, the energized motor causes the pinion to rotate slide out of the abutment position, to reach the moment where the pinion and the ring gear are engaged, then the same process as in the last case follows.

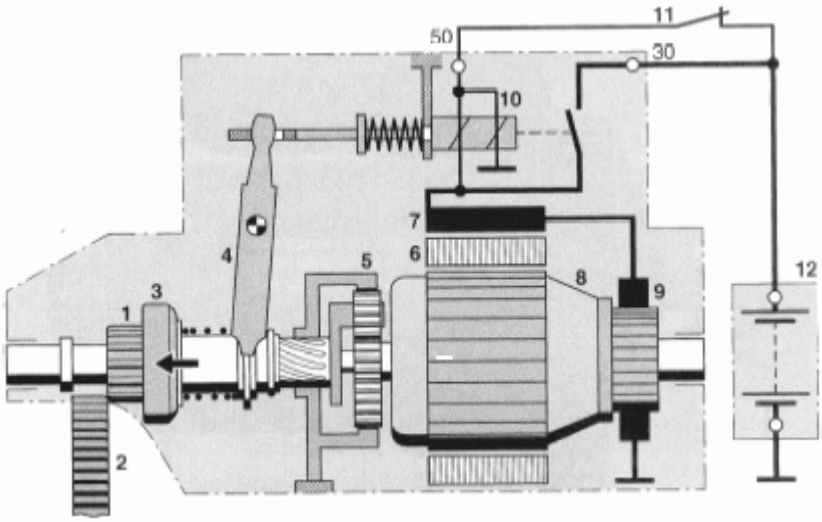

1 Pinion
2 Ring gear
3 Freewheel(overrunning clutch)
4 Engagement lever
5 Planetary gear
6 Pole shoe
7 Excitation winding
8 Armature
9 Commutator with carbon brushes
10 Solenoid switch with pull-in and hold-in windings
11 Starter Switch
12 Battery
13 Electric power supply connection
14 Electric control connection

Figure 3.6: the complete starter motor.

3.5.3 Planetary gear

In order to be able to deliver the high torque required for cold starting, the motor has to be relatively large–and therefore heavy, but the solution comes with the planetary gear since the same torque can be obtained from a smaller and faster – running electric motor with the result that a weight saving of 30…40% can be achieved depending on the model, smaller starter motors

allow the vehicle manufacturer more scope in the design of the engine compartment and / or the placement of other equipment within the vehicle.

The planetary gearing system used in the starter motor has a fixed internal gear, that is the outer, internally toothed ring gear, the sun gear, which is attached to the armature shaft of the electrical motor The planet gear (of which they are normally three) are thus in engagement with both the sun gear and the internal gear. This shown clearly in figure 3.7

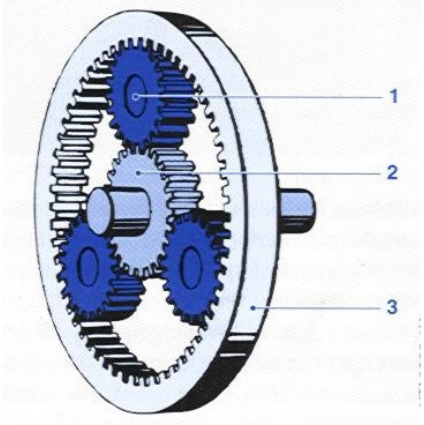

1- Planet gear.
2- Sun gear.
3- Internal gear.

Figure 3.7: Principle of planetary gear.

3.5.4 Solenoid switch

The solenoid switch should be able to switch a high current by means of relatively low control current. The starter motor current can be as high as 1500 A on cars and as much as 2500 A on commercial vehicles.

The solenoid switch built into the starter motor is a combination of a solenoid and a relay switch, it provides the following two functions:

- It moves the drive pinion outwards to finally engage the pinion with the engine's ring gear.
- It closes the switch which completes the starter motor's primary electric circuit

Az it shown in figure 3.8 the solenoid switch consists of:

1. Pull-in winding which is of very low resistance and hence a high current flows. This winding is connected in series with the motor circuit and the current flowing will allow the motor to rotate slowly to facilitate engagement.

2. Hold-in winding which holds the plunger in position as long as the solenoid is supplied from the starter switch.

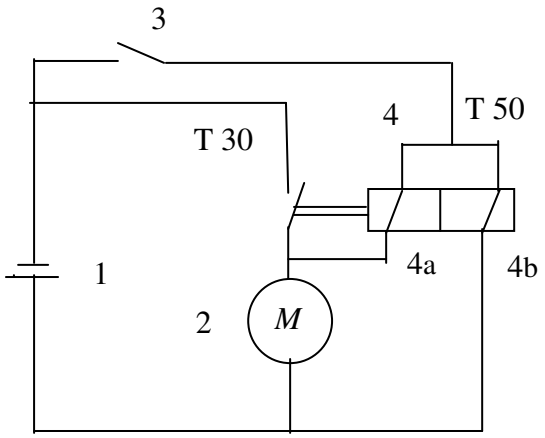

1- Battery.
2- Starter motor.
3- Starter switch.
4- Solenoid switch.
4a- Pull-in winding.
4b- Hold-in winding.

Figure 3.8: Solenoid –switch circuit.

3.5.5 Overrunning clutches

In the starter motor, the drive is transmitted via an overrunning or one-way clutch, which is positioned between the motor and the pinion.

The one-way clutch mission is to transmit the drive to the pinion when the starter motor is driving the ring gear, also to disengage the pinion from the pinion drive shaft as soon as the ring gear is moving faster than the pinion.

The one-way clutch therefore prevent the armature of the starter motor from being accelerated to excessive speeds once the engine has started.

3.6 Temperature dependency

In this section the temperature dependency that will be consider in the model in the next section is summarized.

When the temperature decreases we notice the following changes in the starter itself and in the cable (between the battery and the motor).

- By using the Ceramic Ferrites in the starter motor, and according to the thermal properties of this material, a higher residual flux density (B_r) and thus higher flux (ϕ) ($\phi = BA$) will obtains when the temperature is decreased and that leads to higher generated torque:
  $T_e \sim K_t$ Where $K_t \sim \phi$.

.

- The cable resistance R_c and the armature resistance R_a will decrease when the temperature decrease, as it is shown in Equation (2.4) for the power cable and the same equation will apply for the armature resistance later.

3.7 The model

Modeling and simulation of PMdc motors and thier applications, are complex system that required a great deal of attention to the details and issues involved in these applications.

The model designed by using the Mast Hardware Description Language (HDL) 5.1.

Figure 3.9 shows this model. Port 1 is connected to the battery positive terminal. Port 2 is connected to the ground. Port 3 is connected to the load.

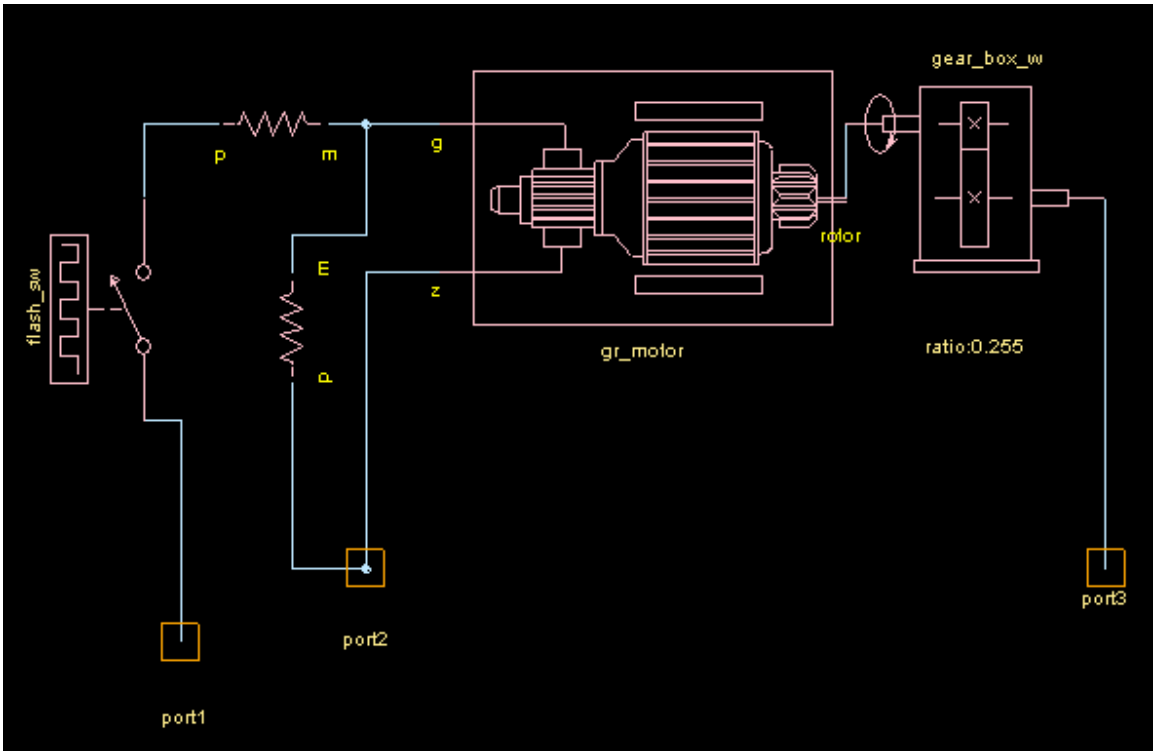

Figure 3.9: The starter motor model.

The simulation consists of physically-based model for starter motor during cranking.

The starter motor dynamics are determined by the motor's characteristic and its effective inertia as seen by the engine.

3.7.1 Effective inertia

The internal gear in the starter motor affect the effective inertia of the starter motor as seen from the engine side, as it illustrate in Figure 3.10.

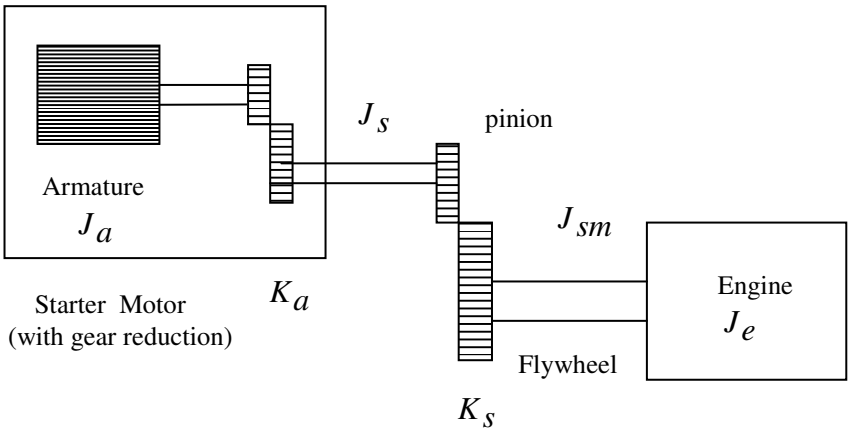

Figure 3.10: Starter Motor Inertia.

The inertia of the starter motor referred to the engine side can be described by:

$$J_{sm} = K_s^2 J_s \tag{3.8}$$

$$J_s = K_a^2 J_a \tag{3.9}$$

$$J_{sm} = K_s^2 K_a^2 J_a \tag{3.10}$$

Where K_s is pinion to flywheel gear ratio, K_a is planetary to internal gear ratio, J_{sm} is the effective starter inertia as seen from the engine.
J_a is the starter motor inertia before the reduction gear.
J_s is the starter motor inertia after the reduction gear.

Thus the add ional gear inside the motor increases the inertia at the motor's output shaft by a factor equal to the square of the internal gear ratio K_a^2.

3.7.2 Starter characteristic

The characteristic of the starter motor can be described as following:

In Section 3.3.2 we found that the generated torque and the induced voltage were given by the following two equations respectively

$$T_e = T_{gen} = K_t I$$

$$E = Emf = K_e \omega_m$$

By using the equations above and with reference to Figure 3.11 the following equations can be derived

$$U_{in} = (R_{br} I + R_a I + R_{sll} I + L_a \frac{dI}{dt}) + Emf \quad (3.11)$$

$$T_q(rotor) = T_e - d\omega_m - Sft - J \frac{d\omega_m}{dt} \quad (3.12)$$

$$T_q(rotor) = T_e - T_{losses} \quad (3.13)$$

Where L_a is the inductance of the armature winding, R_{sll} is the stray load losses resistance and the rest of the parameters in Equation (3.11) are defined in section 3.5.1.
For the torque Equation (3.13), $T_q(rotor)$ is the rotor shaft torque, T_e is the electromagnetic torque, d is motor viscous damping coefficient, Sft is the static friction losses, J is the motor inertia.

Actually the starter motor model basically is based on Equations 3.11 and 3.12. During steady state operation equation these two equations become:

$$U_{in} = (R_{br} + R_a + R_{sll}) I + Emf$$

$$T_q(rotor) = T_e - d\omega_m - Sft$$

By combining equation (3.11) in steady state with $Emf = K_e \omega_m$, we obtain

$$\omega_m = \left[\frac{U_{in} - (R_a + R_{br} + R_{sll})}{K_e} \right] I \qquad (3.14)$$

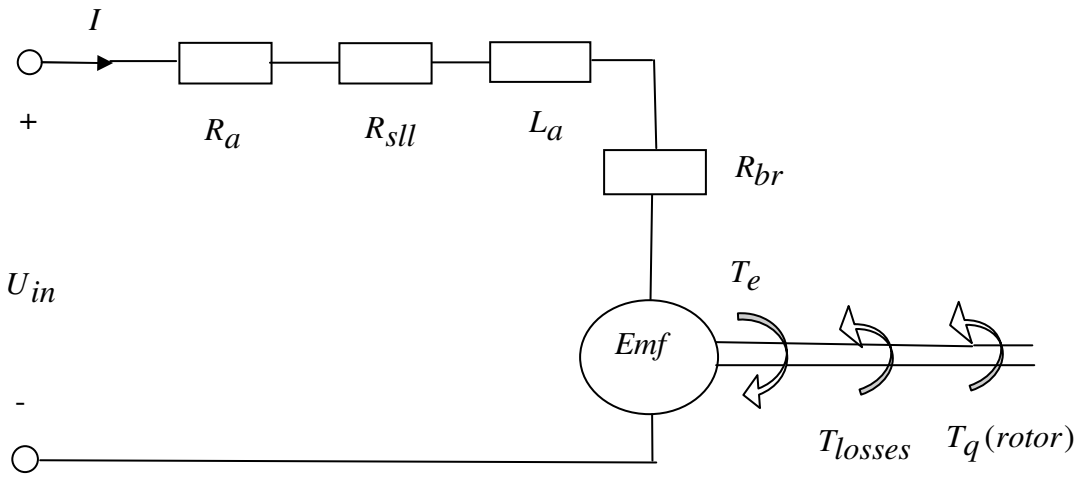

Figure 3.11: Schematic starter motor.

3.7.3 Ke and Kt

In Section 3.3.2 these two constant defined as voltage and torque constants respectively, they are functions of the physical characteristic of the machine.

$$K_e = K_t = \frac{p}{\pi} \Phi T_{se} \quad \text{or} \quad K_e = K_t = \text{constant} \times \Phi$$

In the model K_e and K_t are temperature dependent parameters, in other words *Ke* and *Kt* are proportional inversely to the temperature, the following equation will use to calculate the values of the *Ke* and *Kt* during temperature variation:

$$Ke(t) = Ke(0)(1 - 0.002t) \qquad (3.13)$$

Where $Ke(t) = Kt(t)$ are the desired Voltage (torque) constant at certain temperature (t), $Ke(0)$ is the Voltage (torque) constant at t = 0°C.

In this model the effect of the flux concentration on K_e and K_t will not be taken into account accurately, instead this effect will be estimated experimentally, i.e. K_e and K_t values at no load were tuned, in order to fit the characteristics at no load those supplied by the Bosch.

Then when the starter motor loaded, K_e and K_t will change strongly to the values given by the supplier at full load. While in reality this change should be linearly with increasing the load.

(Notice that K_e and K_t take the lowest values at no load by the flux concentration).

It's important to mention that the expression for determination K_e and K_t provided by Bosch is

$$Ke(t + T_0) = Ke(T_0)(1 - 0.002t) \qquad (3.14)$$

Where T_0 =25°C.
The Equation (3.13) was derived from the last equation in order to make it suitable for implementation in Saber.

Compared values for Ke and Kt based on (3.13) and (3.14) at different temperatures are found in the Appendix.

3.7.4 Solenoid

The solenoid is modeled as a resistance which is connected in parallel to the starter motor model.

By that this model will consider only the Hold-in winding, since the Pull-in winding will shunted off when the starter motor primary circuit is closed, that moment is the start point for our simulation.

The resistance value is provided by the supplier Bosch.

3.7.5 Starter motor inertia

The inertia of the starter motor J is collected in this component, and J value is provided by the supplier Bosch.

The term $J\frac{d\omega_m}{dt}$ in (3.12) is one part of the torque losses.

3.7.6 Planetary (internal) gear

The planetary gear is ideal (no mechanical losses taken into account) and the ratio value is provided by the supplier Bosch.

3.7.7 Losses

The losses determine the heating of the machine and consequently the rating or output power that a machine can produce without that the insulation is subjected to overheating over a reasonable period. Theses losses fall into four basic classes:

3.7.7.1 Static friction (Sft)

Also known as break-away friction, and it consists of cogging (changes in magnetic circuit reluctance), brushes-commutator frictions, and bearing friction at stall within the starter, i.e. it's the torque which needed to overcome to start rotate the starter.

The static friction is modeled as a constant value provide by a supplier Bosch.

3.7.7.2 No-load rotational losses

No-load rotational losses are the sum of mechanical losses plus the no-load core losses.

- No-load core losses consist of hysterises and eddy current losses (iron losses). Time-varying fluxes produce core losses in Ferro magnetic materials, no such losses occur in iron cores carrying flux that does not vary with time.

  The hystersis losses are caused by the resistance of the core material to constant changes of magnetic orientation. The area of the hysterises loop represents the energy loss during one cycle in a unit cube of the core material.

  The hystersis loss per second is commonly expressed by:

$$P_h = K_h (Vol) f B_m^n \tag{3.15}$$

  The definition for all the parameters is found in the list of symbols.

- Since iron is conductor, a changing flux induced voltages and currents called eddy currents that circulate within the iron mass.

  These eddy currents produce losses, heating, and demagnetization and it is expressed by:

$$P_e = K_e (Vol) f^2 \tau^2 B_m^2 \tag{3.16}$$

  To reduce eddy current losses, ferromagnetic material are laminated, and the thin sheets must be oriented in direction parallel to the flow of magnetic flux.

By observing (3.15) and (3.16), it is obvious that P_e is proportional to the squire of the frequency or (speed), while P_h is proportional to the frequency or (speed).

Additional core losses result from harmonic components of flux (such as slot harmonics) harmonics component of mmf. And end leakage flux caused in the

end portions of windings. In fact these additional losses will be included in the stray-losses.

- Mechanical losses are caused by windage, brush friction, and bearing friction during rotor rotation, generally these losses are function of the machine speed.

The core and mechanical losses are modeled together by the term $d\omega_m$ where d and ω_m defined before, d is provided by the supplier Bosch.

3.7.7.3 Armature winding copper losses

These losses are the losses that consist principally of I^2R losses in armature winding, and they modeled as following:
The armature resistance R_a will modeled as a temperature dependent resistance, where the suppler provide R_a at specific temperature equal to 27 °C, and according to (3.17) R_a will change given the corresponding values for different temperature.

$$r(t) = r_{nom}(1 + \alpha(t - t_{nom})) \tag{3.17}$$

where *r(t)* is the resistance at desired temperature, r_{nom} is the resistance at t = 27 °C, *t* is the climate temperature, t_{nom} is equal to 27 °C, and α is the temperature coefficient of the armature resistance where the default value is 0, 0039 for copper material.

3.7.7.4 Brushes losses

The voltage drop in the brushes is a non-linear voltage drop which is similar to a diode drop in an electronic circuit.

it is modeled as a constant resistance which its value is provided by the supplier, thus the voltage drop across the brushes will dependent on the load current.

3.7.7.5 Stray-load losses

These losses arise from the non uniform current distribution in the conductors and the additional core losses produced in the iron by the distortion of the magnetic flux distribution caused by the load current.

It is usually difficult to determine the stray-load losses accurately; estimates are based on test, experience and judgment.

Since these losses are depended on the current, it is modeled as a resistance R_{sll} connected in series with R_a in the starter motor circuit.

The resistance value is adjusted in order to match the values for current, speed and out put power between the simulation results and the characteristic from Bosch.

It is important to notice that R_{sll} are different for different temperatures, since the stray load losses are dependent on the temperature in addition to the current load.

3.7.8 Parameters set up

The parameters those supplied by Bosch are shown in the table below

Armature resistance R_a at t = +20 °C	$R_a = 1{,}754 m\Omega$
Armature winding inductance L_a	$L_a = 4{,}31 \mu H$
Brushes resistance + other connector resistance R_{br} at = +20 °C	$R_{br} = 1{,}666 m\Omega$
Torque and Voltage constant K_e, K_t at t = +25 °C	$K_e = K_t = 7{,}67 mN.m / A$
Motor inertia J	$J = 3{,}92 \times 10^{-4} kg.m^2$
Motor damping constant d	$d = 0{,}4 Nm / radps$
Internal gear ratio K_a	$K_a = 3{,}92$
Hold-in winding resistance	$R_{hold-in} = 1{,}17\Omega$
Ideal (static + dynamic) friction losses $sft + dfl$	$sft + dfl = 0{,}3 Nm$

3.8 The simulation result

The tables 1 and 2 are show the compeered between the simulation and the supplier results at the starter motor for 20°C and -30°C respectively, the reason to chose the simulation at these two temperatures that; the only supplied characteristics from Bosch were at -30°C and +20°C.

Load (N.m)	I(A) Model	I(A) Bosch	Uin (V) Model	Uin (V) Bosch	Pout(Kw) Model	Pout(Kw) Bosch	W(K rpm) Model	W(K rpm) Bosch
20	710	730	8,72	8,6	3,02	2,75	1,44	1,33
15	555	560	9,42	9,4	3,06	2,85	1,95	1,8
10	401	410	10,1	10,2	2,57	2,55	2,45	2,4
5	247	265	10,8	10,8	1,54	1,65	2,95	3,3
0	137	100,5	11,3	11,5	0	0	4,2	5,4

Table 1: The compared results at +20°C.

Load (N.m)	I(A) Model	I(A) Bosch	Uin(V) Model	Uin(V) Bosch	Pout(Kw) Model	Pout(Kw) Bosch	W(K rpm) Model	W(K rpm) Bosch
20	638	610	7	7,3	2,5	2,39	1,19	1,2
15	497	475	8	8,2	2,59	2,52	1,65	1,65
10	357	355	8,9	9	2,2	2,25	2,1	2,2
5	216	230	9,9	9,9	1,34	1,48	2,56	2,9
0	111,7	100,5	10,5	10,8	0	0	3,67	4,4

Table 2: The compared results at -30°C.

In this simulation K_e and K_t values at no load condition were tuned at 6,353 mNm/A at 0°C. While at load condition they sited up at 8,053mNm/A at 0°C, and according to (3.13) they will take different values for different temperatures.

Another parameter were tuned in this simulation it is the stray-load losses resistance *Rsll* = 2, 4 m Ω At T=+20°C. *Rsll* = 1, 3 m Ω at T= -30 °C.

It is clear from this result that the biggest difference between the simulation and measurement results are at no load condition, the speed error is between 17% and 23% and that because of the not accurate values for K_e and K_t at no load condition, In addition to represent the no-load rotational losses by one term $d\omega_m$, while each parts of this losses should be represented individually, as it explained in section 3.7.7.2.

we can see that the compared results for different load values from 5 to 20 Nm are more accurate, the error percent for current, speed, voltage and output power are vary between 1% and 10 % and that because of using more accurate values for K_e and K_t at load condition which supplied by the Bosch.

3.9 Future work

- using a better battery model instead of the simple one we have used will give more accurate result.
- Investigate the effect of the flux concentration of the magnet poles design on the flux (Φ) in the magnetic circuit, and consequently on the torque constant (K_t) at no load.

  This is an important characteristic for further investigation to find an accurate relation between these two parameters (Φ and K_t) by the effect of flux concentration.

- Modeling each parts of the no-load rotational losses individually and investigate the effect of the temperature on them, could help for more accurate model and better result.

- The internal gear was modeled as ideal, a better model could be developing by considering the mechanical losses in the internal gear.

- Taken into account that the brushes drop voltage is a non linear probably give better result.

Chapter 4

The Diesel Engine

4.1 Introduction

Today compression ignited engines are used in a number of different applications, such as cars, boats and power plants. A diesel engine is compression ignited, which means that the rise in temperature and pressure during compression is sufficient to cause ignition of the fuel. The starting process of a combustion engine has two different states. The first one is when the engine is driven by the starter and the other is when the engine has started to run by itself, but have not yet reached a stable idle speed. When the engine has reached idle speed the starting process is finished.

The state when the engine is driven only by the starter is called cranking. The engine model in this report handles cranking.

4.2 Theory

A basic multi-cylinder diesel engine used within the automotive industry, such as the one modeled in this thesis, usually has the following basic design and components as seen in Figure 4.1.

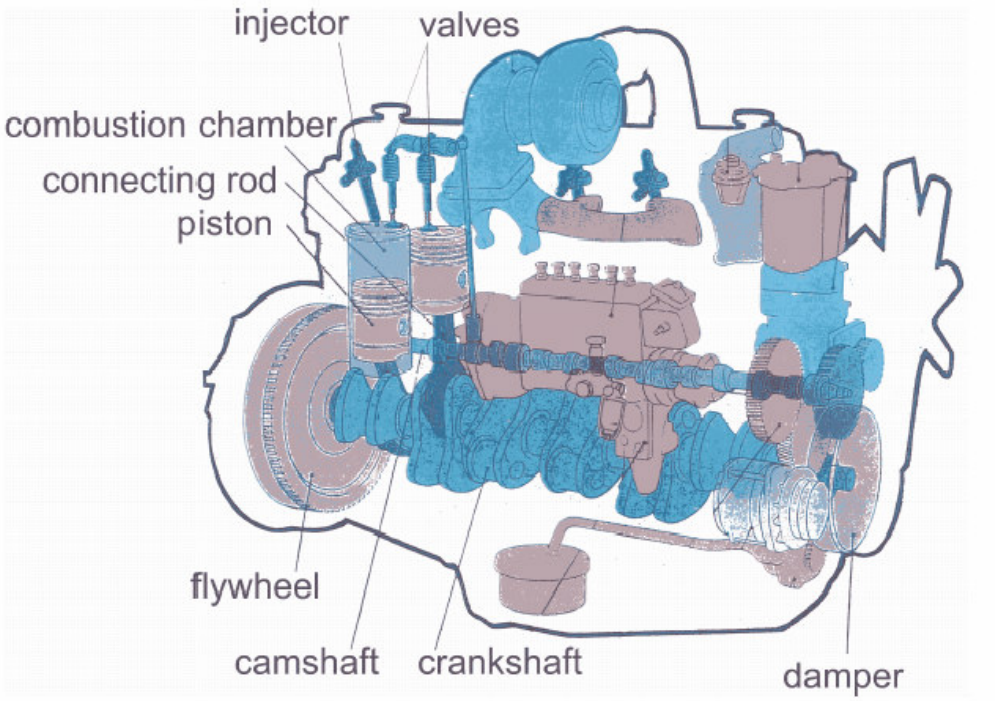

Figure 4.1: Overview over a combustion engine.

The principle behind an internal combustion engine is that air and fuel are mixed and burnt inside the cylinder to generate work. The combustion pushes the piston, which transfer the translational movement through the connecting rod, to a rotational movement on the crank shaft. The combustion process follows four strokes within two revolutions. During each cycle, the piston moves continuously back and forth between its top and bottom positions, commonly known as the Top Dead Center (TDC) and the Bottom Dead Center (BDC), respectively. The crankshaft drives, through a belt, the cam shafts which, in turn, control the valves. The four stroke cycle is divided into the following steps (see Figure 4.2):

Intake *TDC- BDC* ($\theta : 0° \rightarrow 180°$)
The inlet valve opens and air from the intake manifold is inducted into the cylinder. The flow is caused by an underpressure obtained by the increasing cylinder volume as the piston moves downwards.

Compression *BDC- TDC* ($\theta : 180° \rightarrow 360°$)
The inlet valve closes and mechanical work from the crankshaft pushes the piston back towards TDC, compressing the air to create high pressure and high temperature within the cylinder. Fuel is injected into the cylinder before the piston reaches TDC.

Expansion *TDC- BDC* ($\theta : 360° \rightarrow 540°$)
Because of the high temperature and pressure, the air-fuel mixture self-ignites at TDC. This initiates the combustion process, pushing the piston down to BDC. During this step, the main work on the crankshaft is exerted.

Exhaust BDC- TDC ($\theta : 540° \rightarrow 720°$)
The exhaust valve opens and the burnt air-fuel mixture flows out through the exhaust manifold by the pressure differences and by the piston movements.

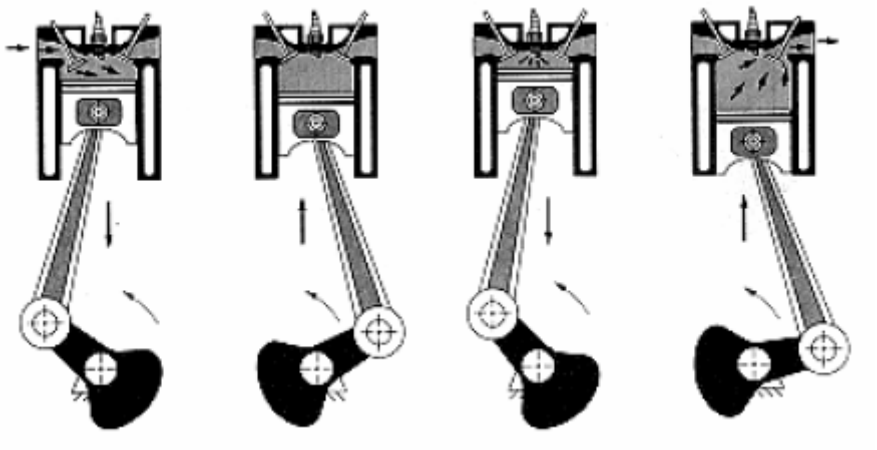

Figure 4.2: The four stroke cycle.

4.2.1 Mechanical losses in a diesel engine

In addition to the moment of inertia of the rotating parts of the engine there are a lot of other mechanical energy losses. The main losses in a diesel engine are due to the compression and to the different friction components, but also the reciprocating inertia by the pistons has an effect. It has been suggested that

the piston ring assembly may be responsible for 50-75 percent of the entire engine friction [**XX**]. The components that contribute to piston assembly friction are the compression rings, the oil control ring, the piston skirt and the piston pin. Other parts have less influence, but in order of importance they are the accessories, the cam bearing friction, the main bearing and oscillatory friction in the valve train.

4.2.1.1 Engine lubrication

Good lubrication is an important way to minimize friction in an engine. There exist three different regimes of lubrication depending on the thickness of the lubricating oil film: boundary, mixed and hydrodynamic. In hydrodynamic lubrication the surfaces are completely separated by the lubricant oil film. In mixed lubrication direct contact between the moving parts occur due to film breakdown and in the boundary regime no oil film exists at all between the surfaces. Engine developers strive for a situation with the lubrication between the mixed and hydrodynamic regimes where the coefficient of friction is the lowest. The Stribeck diagram, as seen in Figure 4.3, is widely used for determining the coefficient of friction.

The viscosity of an oil decreases with increasing temperature. Hence, temperature differences are important to take into account in engine friction calculations.

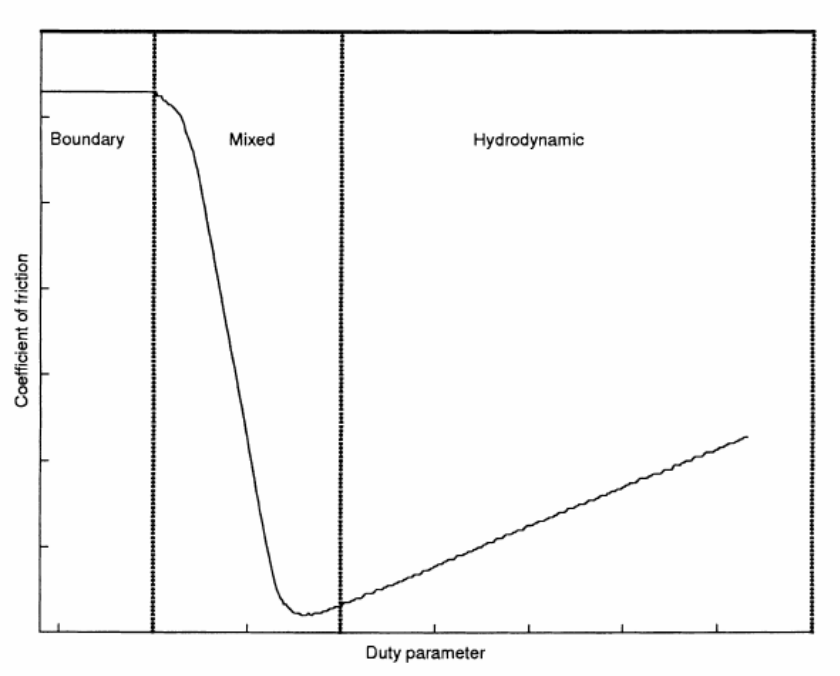

Figure 4.3: The Stribeck diagram.

4.3 Modelling engines

There are numerous ways of describing reality by a model. Some are more complex than others and different approaches taken in modelling can differ greatly in both structure and accuracy. Here follows a summary of the main engine model classifications.

4.3.1 Equations vs. Black Box

Describing the system theoretically by physical equations is the most common method to describe reality. It creates a working model for many operating areas, but has its drawbacks in that it may be difficult to design a correct model and that it is often resource consuming. Another common approach is to base the model only on measurements. The experimental data are stored in a so called black box and then fetched when needed, depending on the input signals. This approach often provides an accurate result, but it is only defined for a limited area.

4.3.2 Mean Value vs. In-Cycle Variation

It is common to simplify a model by regarding all cylinders as equal, and then describe the total engine torque as a mean value over one or more cycles. This approach is called Mean Value Engine Model (MVEM). An alternative method is to describe the torque variations in-cycle. One such example is the Cylinder-by-Cylinder Engine Model (CCEM). Unlike the MVEM, it describes each cylinder individually and takes into consideration instantaneous torques during the cycle.

4.4 The engine model

As mentioned in the introduction is the aim of this thesis to design a comprehensive friction model for the diesel engine NED. The model is constructed in order to predict the behaviour of the engine before starting. Thus, no combustion or fuel injection is considered.

In order to obtain sufficient accuracy, the model is described in-cycle with theoretical equations for each friction component except for the valve train and the oil viscosity models, which are developed from experimental data. All the loss components constitute building blocks in a model describing the entire engine. Most of the fundamental parts of the friction model are based on the theoretical descriptions of Zweiri et al. The derivation of the loss torque of each part and of the engine dynamics are outlined below.

The engine model is implemented in the simulation environment Saber, and all of the components are written in its description language MAST. In Saber it is for layout-reasons useful to make hierarchies, where many components could be grouped under one symbol. It is possible to change parameters outside the hierarchy in the property editor of the symbol. This engine model constitutes of three hierarchical levels.

All model parts have an analogue connection attributing the characteristics of the rotational angle as the across variable and the torque loss of each part as

the through variable. The models of reciprocating torque, compression, piston assembly friction, skirt friction and valve train friction include an output connection as well. The output signal for these ports is the force acting axially on the bearing of the respective parts. Consequently, the bearing friction model has an input to be able to absorb the force. This first approach, though, of the engine model designed in this thesis does not use these in- and outputs for the force since it is simplified to use only hydrodynamic lubrication in the bearings. The hydrodynamic bearing model does not take in to consideration the force acting on the bearing, but the mixed bearing model does.

4.4.1 Loss components

4.4.1.1 Engine dynamics

The dynamics of the system are described by Equation 4.1 and are derived from Newton's principle of a rotational body. $T_{Starter}$ is the input to the engine model in form of the torque generated by the starter.

$$T_{Starter} - T_r - T_{cp} - \sum_{k=1} T_{fk} = J\ddot{\theta} \tag{4.1}$$

The velocity, $\dot{\theta}$, and the angle, θ, of the crank shaft are obtained through integration of its acceleration, $\ddot{\theta}$. T_r, T_{cp} and T_{fk} are engine losses, all outlined below.

4.4.1.2 Reciprocating torque

The reciprocating torque, T_r, is produced by the motion of the piston assembly and the small end of the connecting rod and is described as

$$T_r = MrG(\theta)\ddot{y} = MrG(\theta)\left[G_1(\theta)\dot{\theta}^2 + G_2(\theta)\ddot{\theta}\right] \tag{4.2}$$

where M is the total mass of the piston, the piston rings, the pin and the small end of the connecting rod, respectively, and $\ddot{y}$ is the acceleration of the

reciprocating components. $G(\theta)$, $G_1(\theta)$ and $G_2(\theta)$ are geometrical functions of the engine:

$$G(\theta) = \frac{\sin(\theta+\beta)}{\cos\beta} = \sin\theta + \sqrt{\frac{1-\lambda}{\lambda}}\cos\theta \tag{4.3}$$

where

$$\lambda = 1 - \left[\frac{\delta + r\sin(\theta-\phi)}{L}\right]^2 \tag{4.4}$$

,

$$G_1(\theta) = r\left\{\cos(\theta-\phi)\left[1 + \frac{(r/L)\cos(\theta-\phi)}{\sqrt{\lambda(\theta)^3}}\right] - \sqrt{\frac{1-\lambda}{\lambda}}\sin(\theta-\phi)\right\} \tag{4.5}$$

and

$$G_2(\theta) = r\left[\sin(\theta-\phi) + \sqrt{\frac{1-\lambda}{\lambda}}\cos(\theta-\phi)\right] = rG(\theta-\phi) \tag{4.6}$$

r and L are the crank radius and connecting rod length respectively as can be seen in Figure 4.4, where β, ϕ and other variables are shown as well.

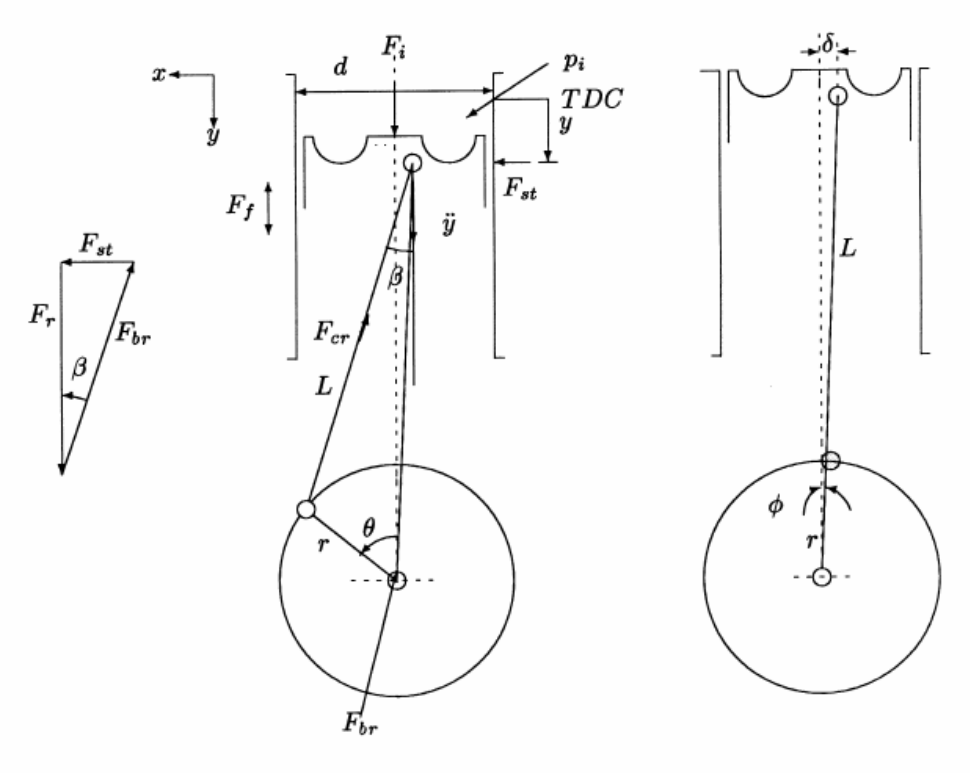

Figure 4.4: Drawing of the crank shaft, connecting rod and piston with some of the variables.

4.4.1.3 Compression

The pressure in the cylinders generates a relatively large torque on the crank shaft which has a prominent effect on the speed variations during cranking.

$$T_{cp} = P_{force} rG(\theta) \tag{4.7}$$

where $rG(\theta)$ is the instantaneous lever. The force P_{force} is expressed as

$$P_{force} = A_p (P_c - P_{atm}) \tag{4.8}$$

where A_p is the exposed area of the piston, P_c the pressure differences in the cylinder pressure, and P_{atm} the atmospherically pressure.

The cylinder pressure varies as the gas mixture in the cylinder undergoes the different phases of the cycle. In this approach the model only takes into consideration the torque influenced during the period where the cylinder is closed, from intake valve closing (θ_{ivc}) to exhaust valve opening (θ_{evo}). The pressure during the remaining period of the cycle as well as the air flow in and out from the cylinders is neglected due to the relatively low speed of the engine during cranking.

From intake valve closing until top dead centre, the gas mixture in the cylinder is being compressed and from top dead centre until exhaust valve opening is it expansioned. While, in this thesis, it is assumed that the cylinder is totally closed during the compression and the expansion and due to the fact that there is no combustion, these two phases are modelled as one. The cylinder pressure P_c is then described by a polytrophic process while the intake and exhaust valves are closed:

$$P_c = P_{atm}\left(\frac{V_0}{V}\right)^{\kappa} \tag{4.9}$$

where κ is a polytrophic index, V_0 is the cylinder volume at the moment where the intake valve closes and V is the instantaneous cylinder volume. The cylinder volume is described as a function of the crank angle θ_i:

$$V = \frac{V_d}{C_{Ratio}} + \frac{\pi d^2}{4}\left[\sqrt{(r+L)^2 - \delta^2} - \left\{\sqrt{L^2 - [\delta + r\sin(\theta_1 - \phi)]^2} + r\cos(\theta_1 - \phi)\right\}\right] \tag{4.10}$$

where V_d is the displacement volume, C_{Ratio} is the compression ratio and d is the piston diameter.

While any of the valves are open the cylinder pressure is assumed to be equal to the atmospheric pressure:

$$P_c = P_{atm} \tag{4.11}$$

4.4.1.4 Friction model

4.4.1.4.1 Piston assembly

4.4.1.4.1.1 Piston rings torques

The piston assembly friction is dominated by the ring friction components. It has been observed that the ring assembly lubrication mode is hydrodynamic except near the top and bottom dead centre positions where the oil film breaks down. The assembly friction torques can be found by assuming that the friction force is equal to the product of the normal load between the ring assembly and the liner, and the friction coefficient. The forces acting on the ring assembly include the static ring tension, the gas pressure force and inertia force. Thus the ring assembly friction torque can be expressed as [zweiri]

$$\begin{aligned} T_{f1} = \eta r \left|G(\theta)\right| \Bigg\{ & \sum_{i=1}^{N} F_{r_i} \\ & + \sum_{i=1}^{N} a_i \left| p_c - p_{atm} \right| * \pi * d_r B_i \\ & + \left[\frac{\left| p_c - p_{atm} \right| * \pi / 4 * d \quad - M G_1(\theta) \dot{\theta}^2}{\eta + G_3(\theta)} \right] \Bigg\} \end{aligned} \tag{4.12}$$

where F_r is the ring force, d_r the piston ring diameter and B_i the width of each piston ring. The geometrical equation is described as

$$G_3(\theta) = \frac{L\sqrt{1 - \{[\delta + r\sin(\theta - \phi)]/L\}^2}}{\delta + r\left|\sin(\theta - \phi)\right|} \tag{4.13}$$

The coefficient of friction for hydrodynamic lubrication, η, is directly proportional to the piston speed and oil viscosity and inversely proportional to the ring load For the coefficient of friction with mixed lubrication, the variation can be approximated by the following equation [zweiri]

$$\eta = \begin{cases} c_1 - (c_1 - z)|\sin\theta| & for \quad x_1\pi \le \theta \le x_2\pi \\ z & otherwise \end{cases} \tag{4.14}$$

where c_1 is a constant and z is the hydrodynamic friction coefficient given by

$$z = \sqrt{\frac{\mu\dot{\theta}r|G(\theta)|}{L_r}} \tag{4.15}$$

and L_r is the load per unit length given by

$$L_r = \sum_{i=1}^{N}\left[\frac{F_{r_i}}{\pi d_r} + (P_c - P_{atm})\right]B_i \tag{4.16}$$

This derivation is assumed to be valid in the system modelled in this study.

4.4.1.4.1.2 Skirt friction

The piston skirt profile is designed to prevent local contact due to thermal expansion and to reduce friction losses and piston slap, by ensuring that a proper lubrication oil film thickness is maintained. The piston skirt friction is derived by applying Newton's law for viscous friction and can be described as [Xx]:

$$T_{f2} = \left[\frac{\mu\dot{\theta}G(\theta)}{O_c}\right]dL_s rG(\theta) \tag{4.17}$$

where O_c is the oil clearance and L_s is the piston skirt length.

4.4.1.4.2 Bearings

The bearings in the engine can be analysed using Reynold's approximation to the Navier-Stokes equations (zweiri). The bearings are treated as axisymmetric and two-dimensional to account for their finite length. The bearings generally operate in the hydrodynamic lubrication regime except around top dead centre. In this thesis, though, the bearing model is assumed to act in the hydrodynamic lubrication regime only.

4.4.1.4.2.1 Hydrodynamic lubrication

By solving the Reynold's equation, Zweiri describes the instantaneous friction torque during hydrodynamic lubrication mode on the bearing as

$$T_{f3} = \left[\frac{F_t \varepsilon}{2} + \frac{2\pi\mu\dot{\theta} r_b^3 L_b G_4(\theta)}{\sqrt{c_r^2 - \varepsilon^2}} \right] \tag{4.18}$$

In this work the bearing eccentricity ε and the geometrical function are neglected and the eccentricity can therefore be seen as set to zero. Consequently, the simplified friction torque can be described as

$$T_{f3} = \left[\frac{2\pi\mu\dot{\theta} r_b^3 L_b}{c_r} \right] \tag{4.19}$$

where μ is the dynamic viscosity of the oil, r_b and L_b are the bearing radius and length respectively and c_r is the radial clearance in the bearing.

4.4.1.4.2.2 Mixed lubrication

Although this model does not include mixed lubrication, it is prepared to do it. As mentioned above, the bearing model has an input for the tangential forces, F, acting on the bearing. The generated torque is described as

$$T_{f4} = \eta_{bm} r_b |F| \tag{4.20}$$

where η_{bm} is the friction coefficient of the bearing during mixed lubrication.

4.4.1.4.3 Valve train

The valve train carries high loads over the entire speed range of the engine. Loads acting on the valve train at lower speeds are primarily due to the spring forces for the valves. The valve train friction is this model is not described by physical equations but is fitted from empirical data. The data is obtained from the engine department at Volvo Car Corporation and represents the torque on the cam shaft produced by a single valve lift. To achieve an expression describing this, a “curve fitting” program was used. The curves are shown in Figure 4.5 where the thin line represents the measured curve and the thick describes the estimated in form of a fifths degree polynomial equation.

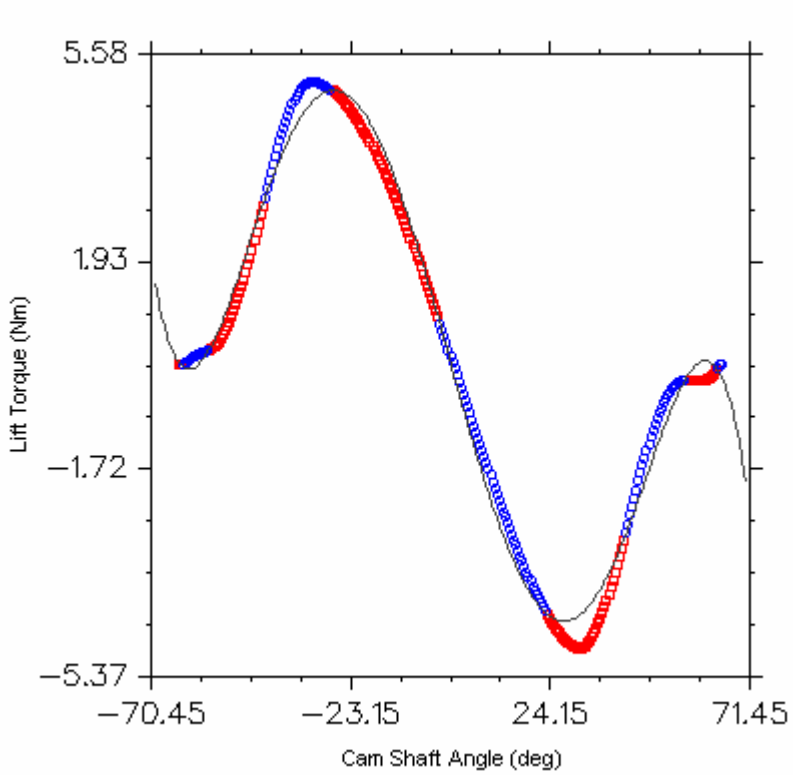

Figure 4.5: Measured and modelled valve train torque.

4.4.1.4.4 Auxiliaries

The only auxiliary modelled in this approach is the oil pump. The description used is taken from Zweiri and it is assumed to be valid:

$$T_{f6} = \sqrt{\mu\dot{\theta}} \tag{4.21}$$

4.4.2 Model construction

As mentioned above, the entire model is built with all the components described above as building blocks. The engine model consists of three hierarchy levels where the level under the top level symbol contributes the

entire engine which can be seen in Figure 4.6. It consists of a crank shaft model docked with five cylinder models, an auxiliary model and a gear model which models the transmission of the cam belt and is assumed to have 100 % efficiency. After the cam belt model follows two units of the cam shaft model and ten of the valve train, one for each inlet- and exhaust valve respectively. The crank- and cam shaft models and the cylinder model are symbols in the bottom level of the hierarchy consisting of different loss components. These three models are described below in the model parts section.

The engine model has one analogue rotational port, contributing the crank shaft of the engine, which has the torque as the through variable and the rotational velocity as the across. In connection with the port a gear model is put to model the pinion to flywheel gear. Due to the fact that all the other components in the engine model uses angle as through variable, a converter is used between the pinion to flywheel and the rest of the parts.

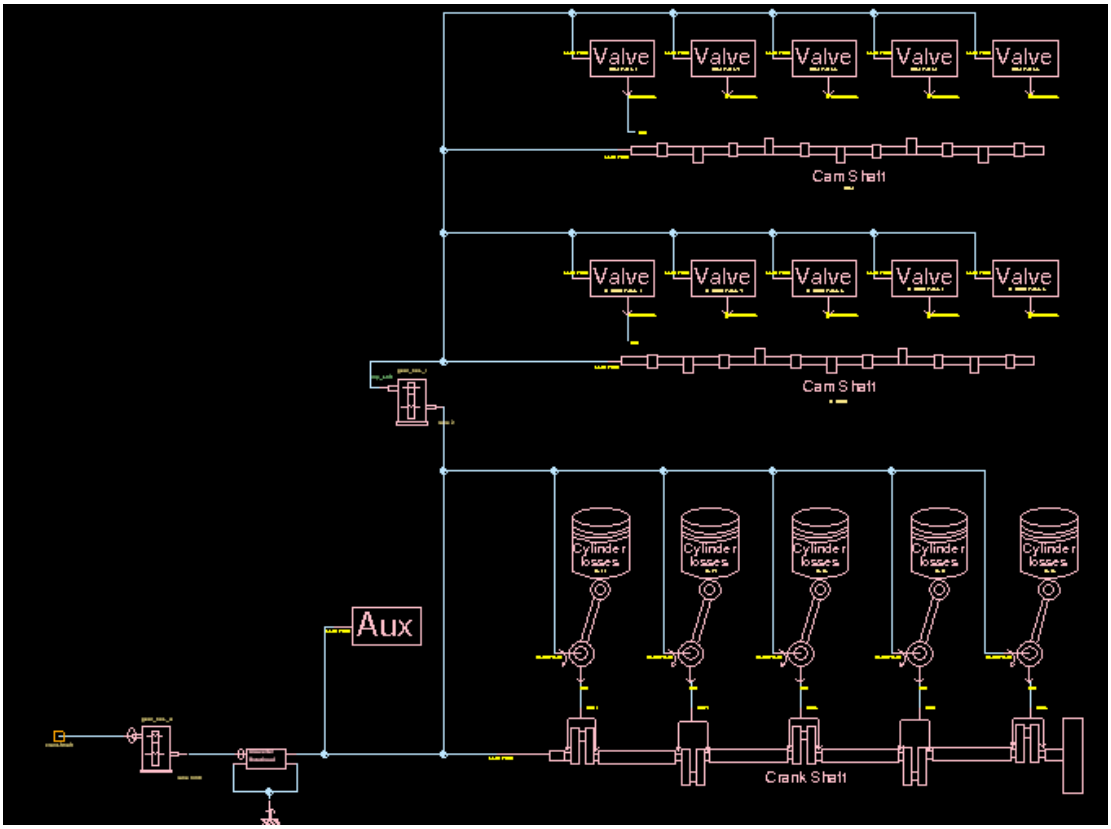

Figure 4.6: The basic structure in the engine model.

4.4.2.1 Model parts

4.4.2.1.1 The crank shaft model

The crank shaft is built with the engine dynamics model as the basic part. This controls the dynamics of the entire model in respect of the sum of all torques acting on the shaft. The crank shaft model also includes one model per bearing, i.e. six in total, regarding the main bearings in the modelled engine.

The interface of the crank shaft consists of one rotational connection and five input ports where the signals from the cylinders forces are received. The forces, produces by each cylinder, acting axially on the bearings are simplified in this approach to affect only the two bearings which are closest to the specific cylinder. That is solved through dividing the signal of each cylinder's

force by two and split it before acting on the bearings. The four bearings in the middle of the crank shaft are affected by two cylinders each and therefore are the force signals from these summarized as well.

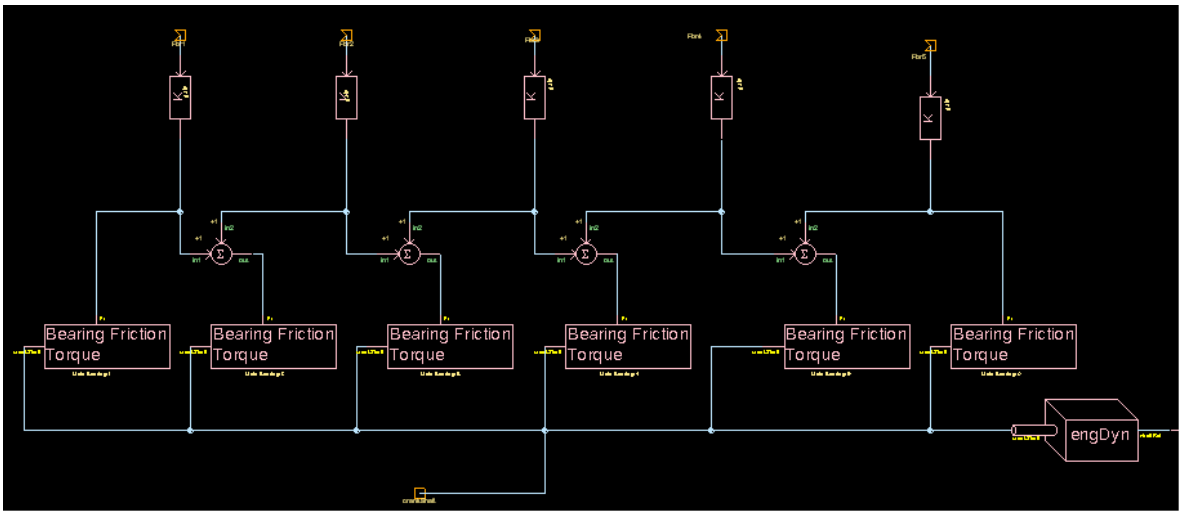

Figure 4.7: The crank shaft model.

4.4.2.1.2 The cylinder model

The cylinder friction model consists of models of ring-, skirt- and bearing friction, reciprocating torque and cylinder pressure torque. The bearing model contributes to friction from the connecting rod bearing, while the piston bearing friction is neglected in this thesis. The force signals from the outputs of the other four models are summarized before partly affecting the bearing model and are partly converted to an output from the cylinder model. The other connection, as can be seen in Figure 4.8, is a rotational port conveying the torques produced by the cylinder parts to the crank shaft.

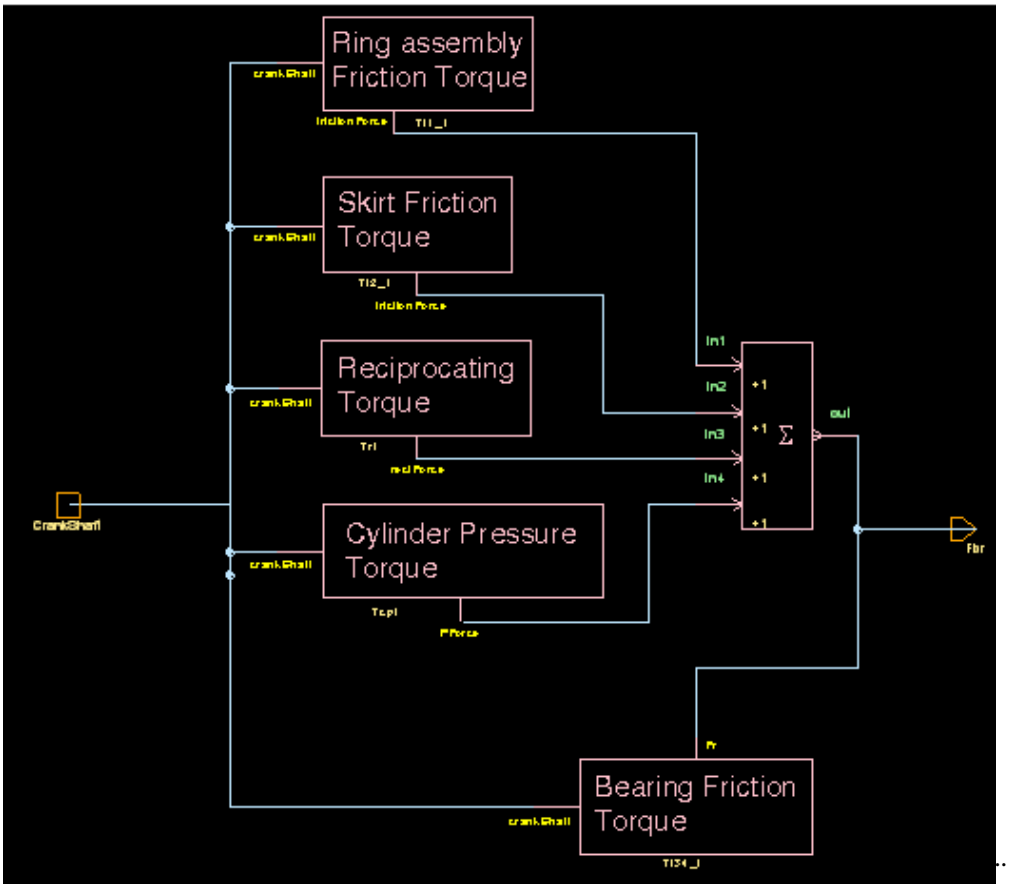

Figure 4.8: The cylinder model.

4.4.2.1.3 The cam shaft model

With the exception of the engine dynamics model is the cam shaft modelled in the same way as the crank shaft with six bearing models, five inputs and one rotational connection.

4.4.3 Temperature dependence

The only temperature dependent behaviour considered in the model is the viscosity of the oil. The oil used in the NED engine is called A99067PBD (Castrol). The following equation is used to describe the viscosity of this oil

as a function of temperature (obtained from the engine department at Volvo (Bertil Andersson)):

$$\mu = A_{oil} e^{\frac{B_{oil}}{C_{oil}+t}} \qquad (4.22)$$

where A_{oil}, B_{oil} and C_{oil} are constants and t is the temperature of the oil.

4.5 Further work

This thesis describes a first approach of the engine losses model. The model is not validated with measured data and it has to be improved in some ways. Recommendations for further developers can be seen below:

- Validate all the different loss component models individually.
- Investigate if the coefficient of friction for hydrodynamic lubrication in the piston ring model is valid for this approach.
- Evaluate if it is a correct assumption to assume only hydrodynamic lubrication for the bearings.
- Model the piston bearing, if it is necessary.
- Evaluate the efficiency of the cam belt and pinion to flywheel gear models.
- Model the oil pump in a better way if it is necessary
- Evaluate if there are any parameters besides the oil viscosity which affects the engine friction due to temperature dependencies.
- Validate the entire engine model.

Chapter 5

Starter system

5.1 Theory

5.1.1 Engine starting requirement

An internal combustion engine requires the following criteria in order to start and continue running:

- A combustible mixture of air and fuel.
- A compression stroke.
- A form of ignition.
- The minimum starting speed (about 100 rev/min).

In order to produce the first three of these criteria, the minimum starting speed must be achieved. This is where the electric starter comes in. The ability to reach this minimum speed is dependent on a number of factors:

1. Rated voltage of the starting system.
2. Lowest possible temperature at which it must still be possible to start the engine. This is known as the starting limit temperature
3. Engine cranking resistance. In other words the torque required to crank the engine at its starting limit temperature.
4. Battery characteristics.
5. Voltage drop between the battery and the starter.
6. Starter -to- ring gear ratio.
7. Characteristics of the starter motor.

One of the important considerations in relation to engine starting requirements is the starting limit temperature. As seen in Figure 5.1, when the temperature decreases, the starter torque also decreases and the torque required cranking the engine to its minimum speed increases.

Typical starting limit temperature for passenger cars is from - 18°C to - 25°C but it reaches - 30°C at some places like in the Scandinavian or in Canada.

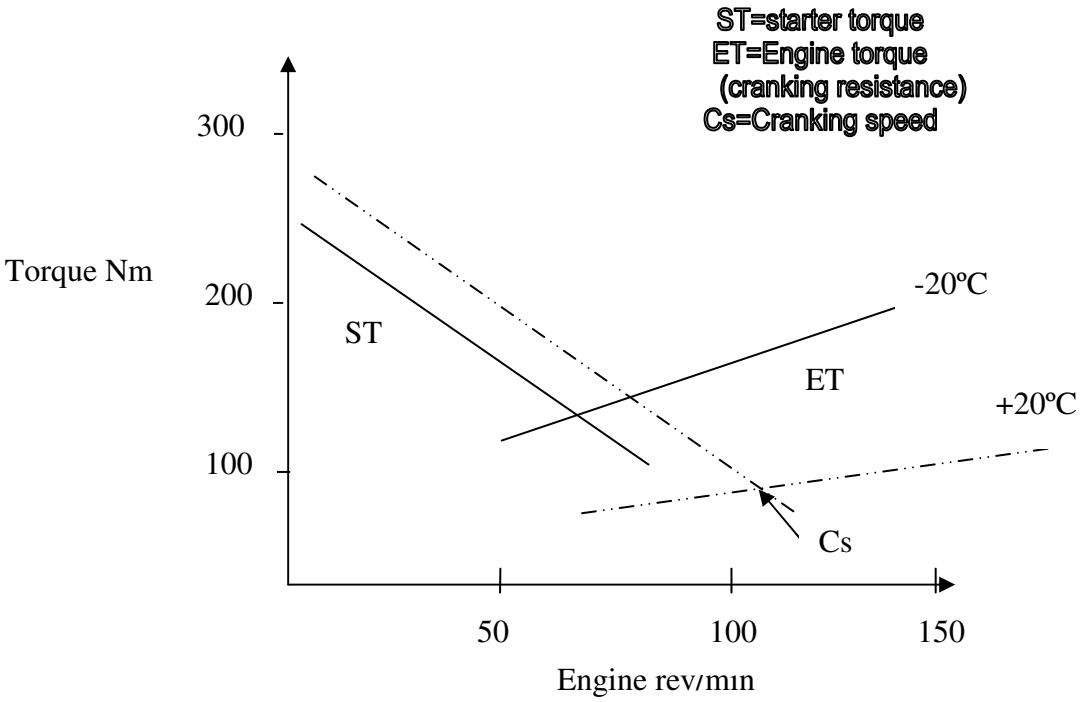

Figure 5.1: Starter torque and engine cranking torque

5.1.2 Starting system design

It is important to determine the minimum cranking speed for a particular engine. This varies considerably with the design and the type of the engine. The rated voltage of the system for passenger cars is, almost without exception, 12V. A battery of maximum capacity for the starter, which has a 20% drop in capacity at - 20°C , is connected to the starter by a cable with a resistance of 1 mΩ. The rated power of the motor corresponds to the power

drawn from the battery minus the copper losses (due to the resistances of the circuit), the iron losses (due to eddy currents being induced in the iron parts in the motor) and the friction losses.

There are two other important considerations when designing the starter system .

The location of the starter on the engine is usually pre-determined, but the position of the battery must be considered. Other constraints may determine this, but if the battery is closer to the starter the cable will be shorter. A longer run implies that a cable with a greater cross-section is needed to ensure a low resistance.

5.1.3 The process of cranking

The torque provided by the starter motor at the beginning of the starting sequence initially overcomes the static friction in the engine and then accelerates the engine to the "turnover speed". This speed is characterized by the engine and the starter motor torque curves and must be above the "minimum starting speed" in order to ensure successful starting. As soon as the cylinders fires, the internal combustion engine start to generate its own torque, though not necessarily enough to start the engine in every case, the starter motor must continue to assist the engine to reach the "minimum starting speed". The various phases of the starting sequence are illustrated by the diagram in Figure 5.2.

The degree of frictional resistance that has to be overcome is heavily dependent on the viscosity of the engine lubricant and thus also on engine temperature. Further more, the required minimum engine speed increases as the temperature decreases. Consequently, the starter motor must produce significantly greater power output for cold starting as compared to when the engine is warm. For this reason, the engine can only be successfully started at temperatures above certain one referred to as the "minimum starting temperature".

The combination of required torque at minimum starting temperature and minimum starting speed provides the required starter – motor power out put, which is the initial criterion for selection of starter-motor type.

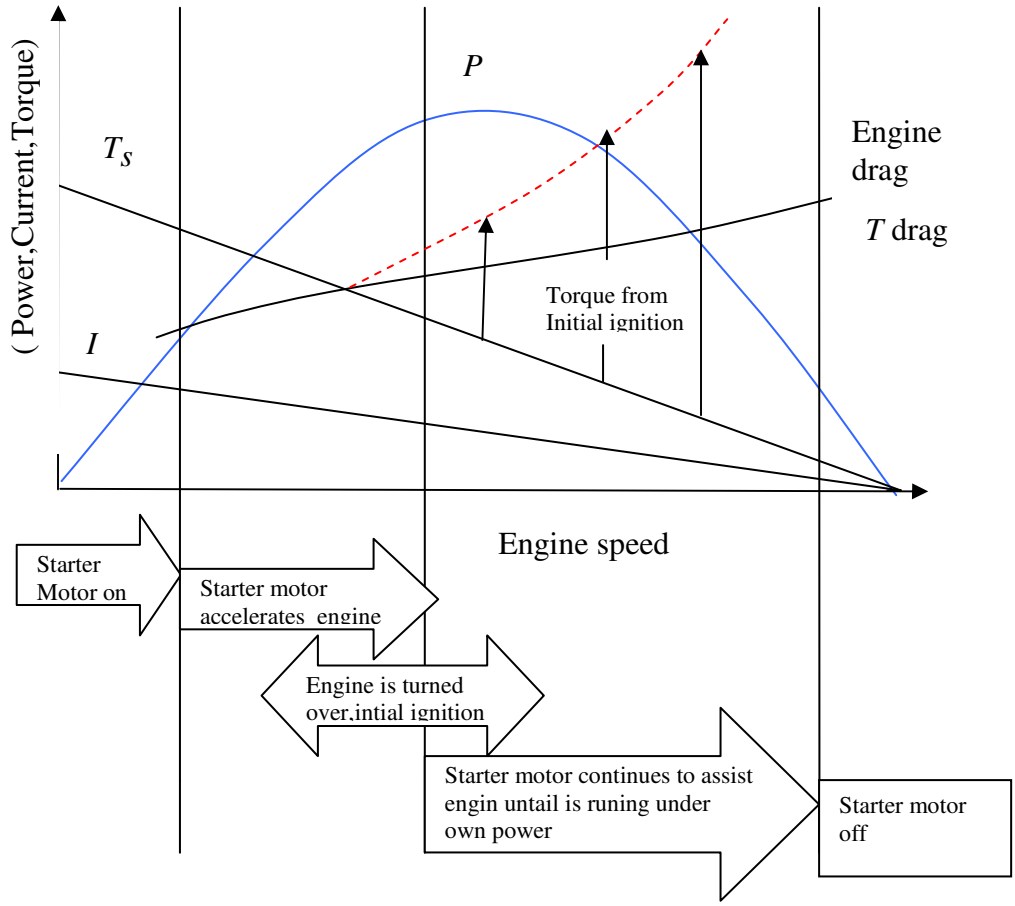

Ts strater –motor torque

T drag Engine drag

P power

I current

Figure 5.2: Phases of the starting sequence.

5.2 Model

The starter system model is based on an assemblage of the models for the battery, the power cable, the starter motor and the diesel engine. The basic structure for the model of the system can be seen in Figure 5.3.

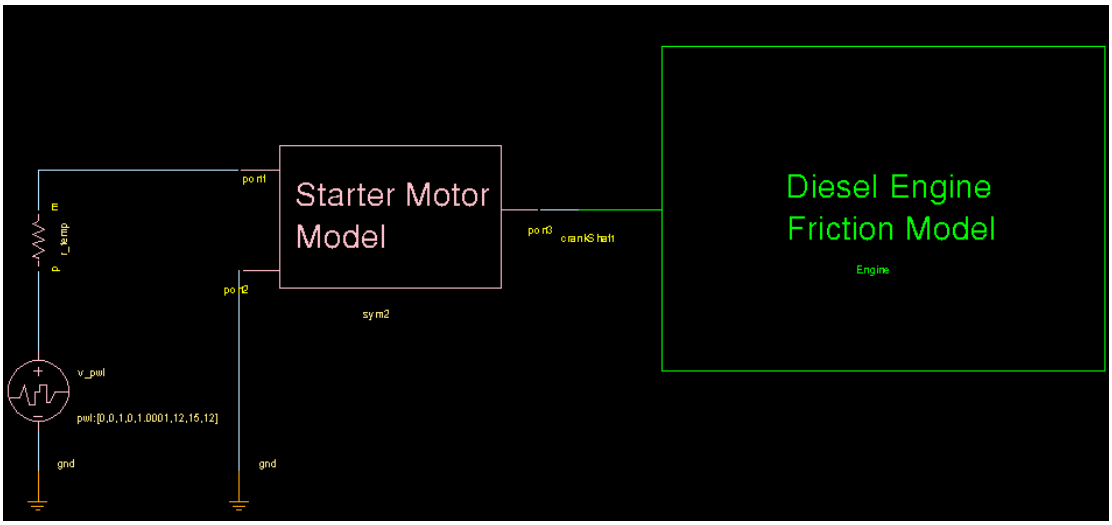

Figure 5.3: The basic starting system model.

5.3 Simulation

5.3.1 Simulation achievement

The starter system model was simulated in Saber for different temperatures between - 30°C and + 60°C. The simulations were made with transient analysis and the simulation time was chosen to 20 seconds since all the results were reach stable values for that time.

To match the set up of the measurements, three aspects have been considered in the simulations:

- The input voltages for the simulation model were set up according to the measurements voltages from the battery since the appropriate model for the battery was not available.

- The solenoid resistance was omitted in the starter model since it was fed separately in the measurements.
- All auxiliaries except for the oil pump were omitted in the engine model since the auxiliary belt was removed in the measurements.

5.3.2 Simulation results

The simulation result for the engine speed at 22°C is around 200 rpm while it is around 130 rpm with higher oscillations at the lower temperature, as seen in Diagrams 5.1 and 5.2.

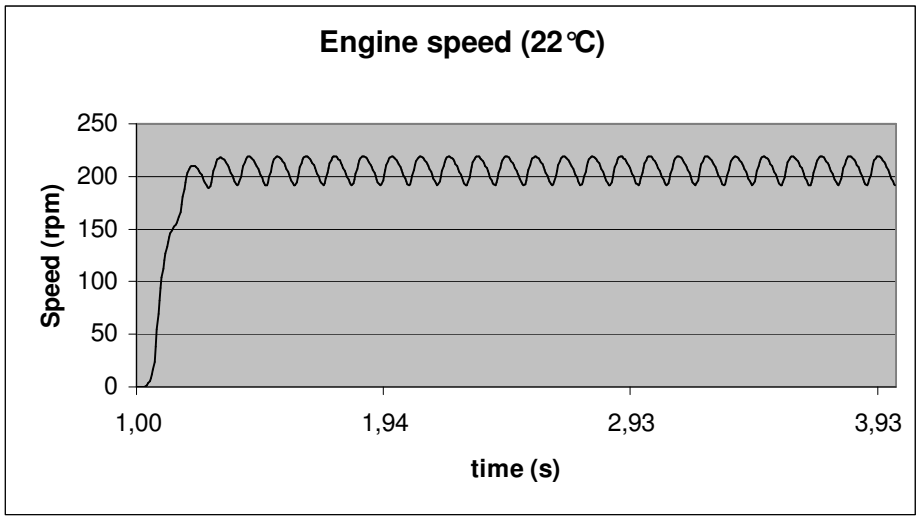

Diagram 5.1: The simulated cranking speed at 22°C.

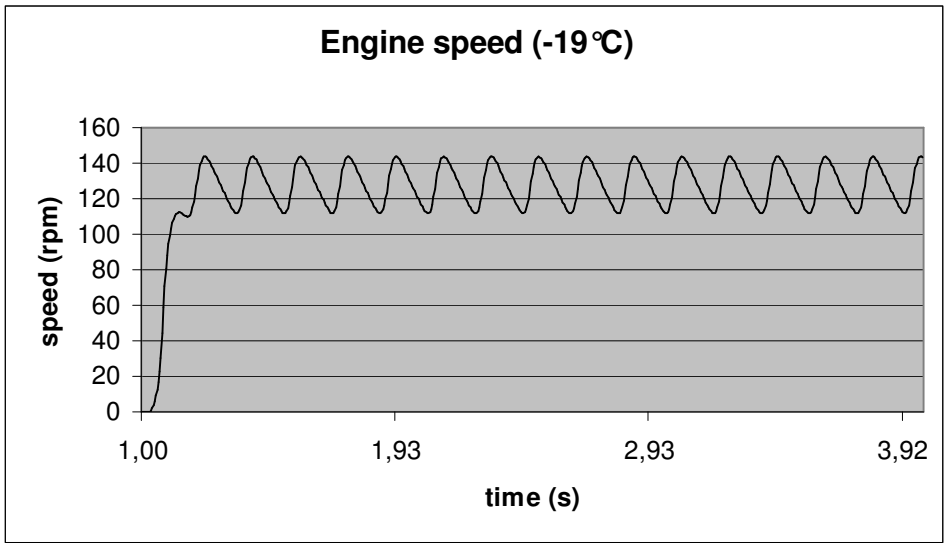

Diagram 5.2: The simulated cranking speed at -19°C.

The simulations result for the starter current at 22°C is, after reaching 1600 A as a peak value, oscillating around 100 A. At the lower temperature the oscillations are higher and the current is around 450 A while the peak value reaches 1700 A. The results for the current simulations can be seen in Diagrams 5.3 and 5.4.

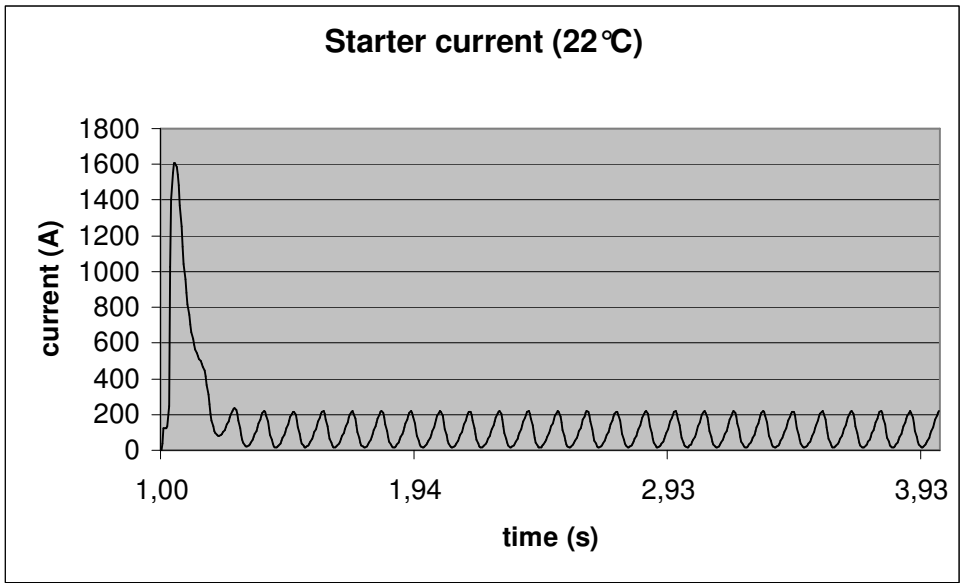

Diagram 5.3: The simulated starter current at 22°C.

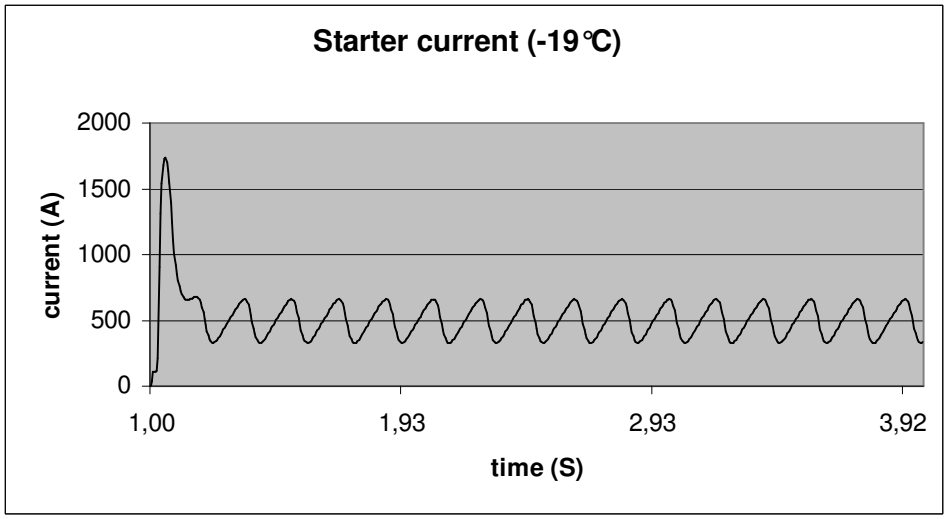

Diagram 5.4: The simulated starter current at -19°C.

The engine model calculates the loss torque individually for each components. Some of these simulation results are shown below:

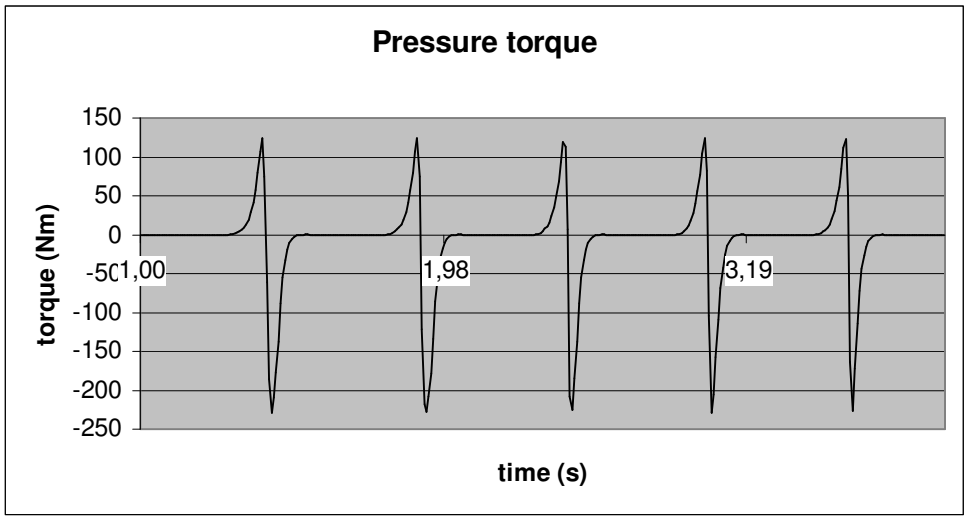

Diagram 5.5: The simulated compression torque for one cylinder.

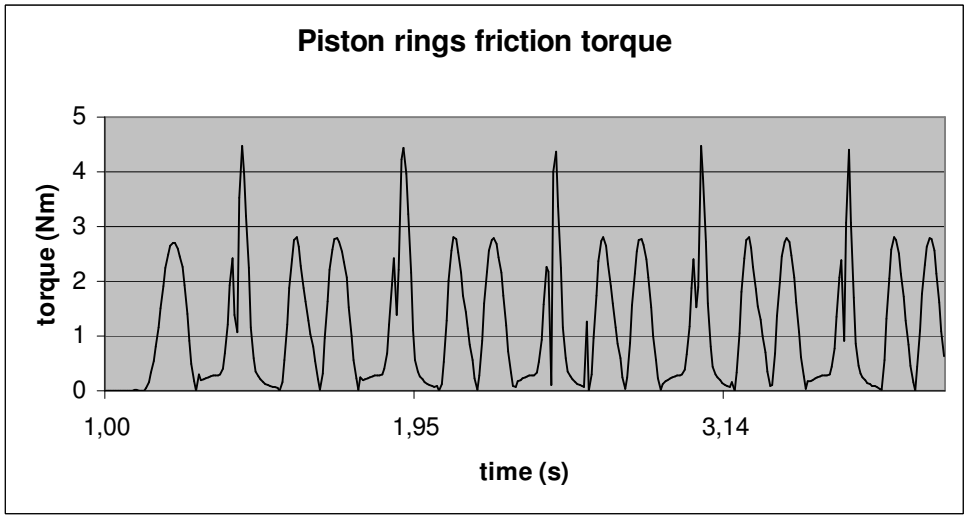

Diagram 5.6: The simulated piston rings friction torque for one piston.

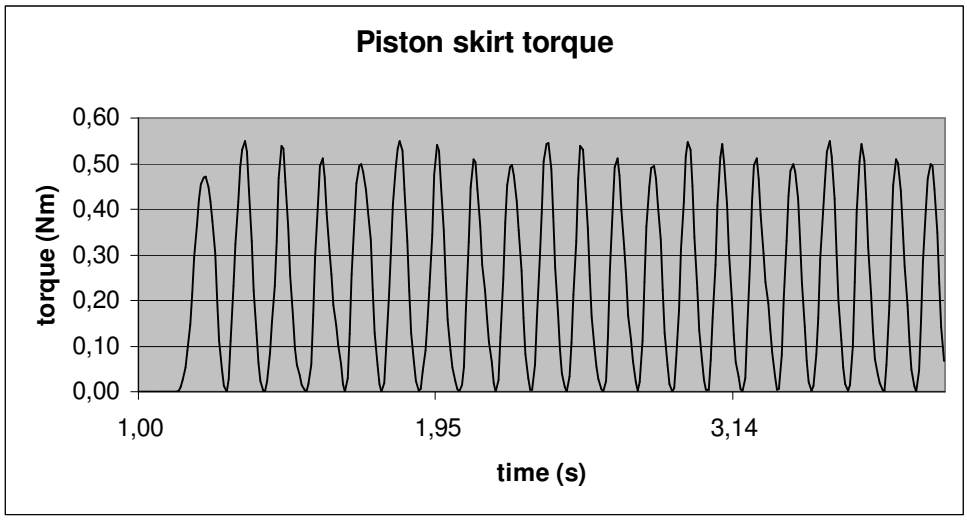

Diagram 5.7: The simulated piston skirt friction torque for one piston.

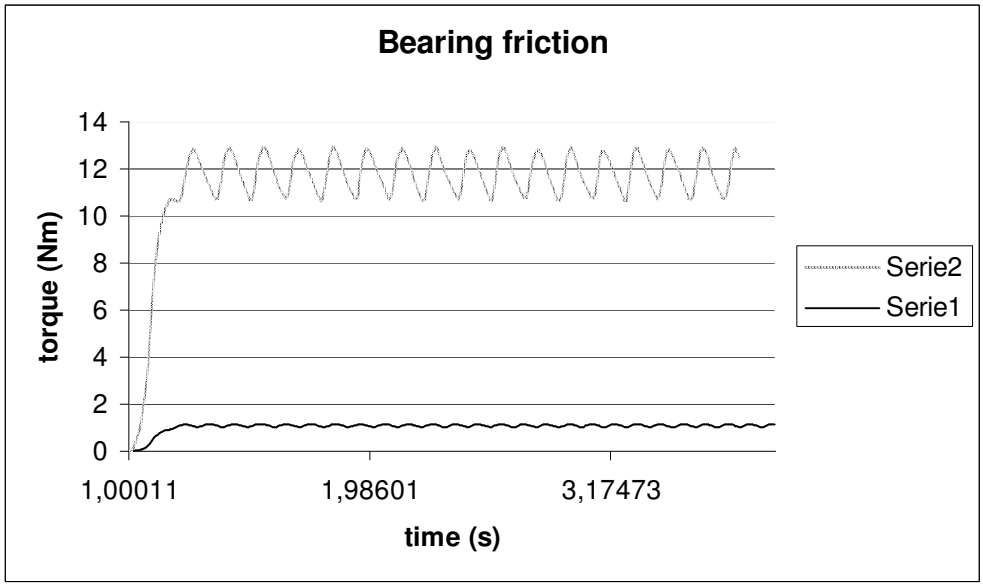

Diagram 5.8: The simulated bearing friction torque at 22°C (Serie 2) and at -19°C (Serie 1) for one main bearing.

Chapter 6

Measurements

6.1 Introduction

One part of the thesis was to make measurements of the cranking system for different temperatures. The aim of this was to measure the starter motor current and input voltage, the voltage on the battery terminals, the temperature of the system, and finally the velocity of the engine's crankshaft.

6.2 Equipment

The measurements were performed on a diesel engine of the type NED and took place in a climate chamber, which operates between - 40°C and + 90°C, at Volvo Car Corporation. The starter was of type R78-M45 from Bosch and for supplying the starter a fully charged H7, 80 Ah, 700 A(SAE) battery was used.

For achieving the measurements we used voltmeters and amperemeter for the voltages and current. For the velocity measurement of the crank shaft a light pulse counter with a signal converter from AVL was used. To convert the signals from the equipment mentioned above to fit the computer software three boxes from Ipetronik called SIM Thermo, SIM CNT and SIM DMS. The software used to collect the data is called ComTest VMD by Mandator and it declares the results in Excel documents.

A total list of the used equipment with its type description and specifications can be found in Appendix X.

6.3 Experimental

A scheme of the set up of the measurement can be seen in Figure 6.1.

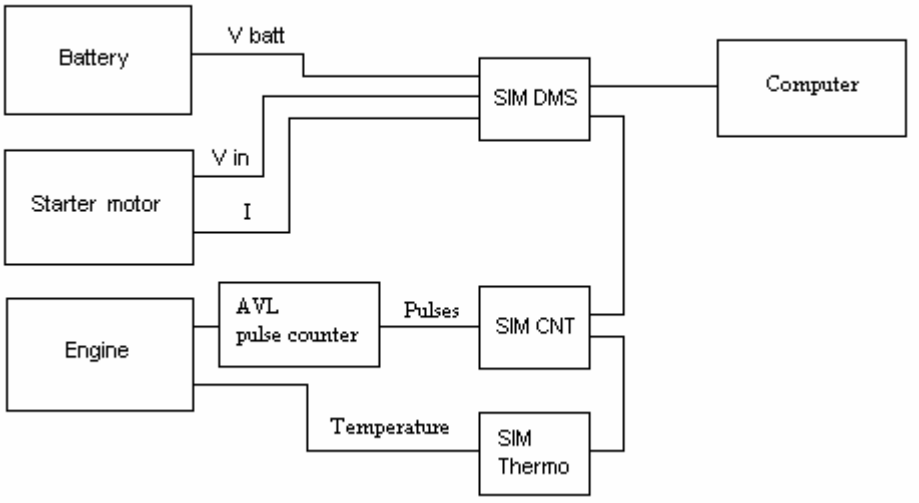

Figure 6.1: Scheme of the measurement set up.

To simplify the modelling of the engine the auxiliaries except the oil pump were disconnected by removing a belt from the engine. The solenoid was fed by a separate battery while in the actual cranking system it is supplied by the same battery which feeds the starter motor.

6.4 Measurement results

The measurements are done at several temperatures: - 30°C, - 25°C, - 19°C, - 10°C, 0°C, + 22°C, + 40°C and + 60°C. In the Figures below the results at + 22°C and - 19°C are shown.

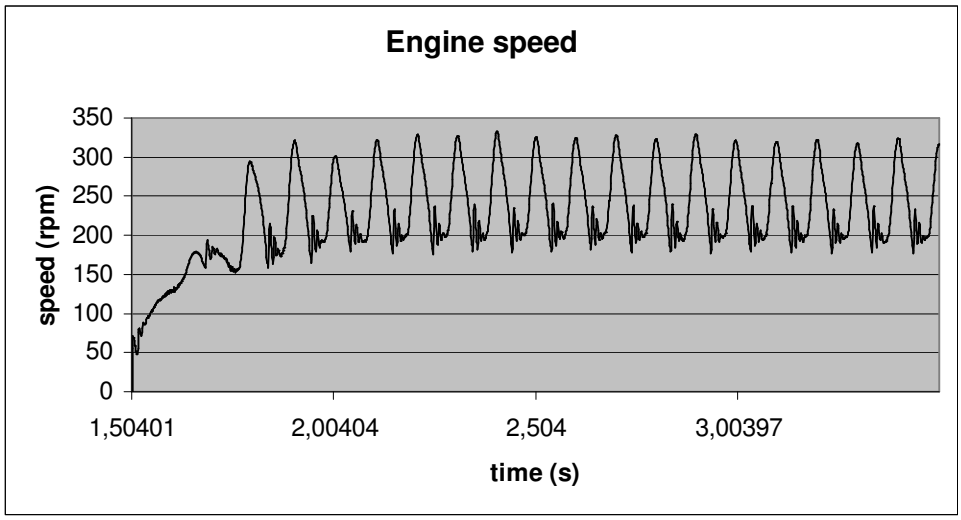

Diagram 6.1: Measured engine speed at 22°C.

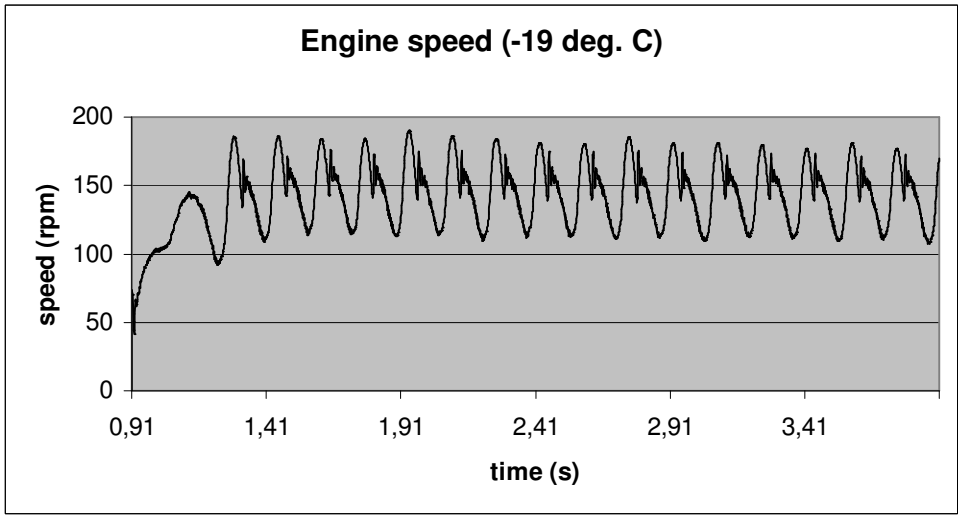

Diagram 6.2: Measured engine speed at -19°C.

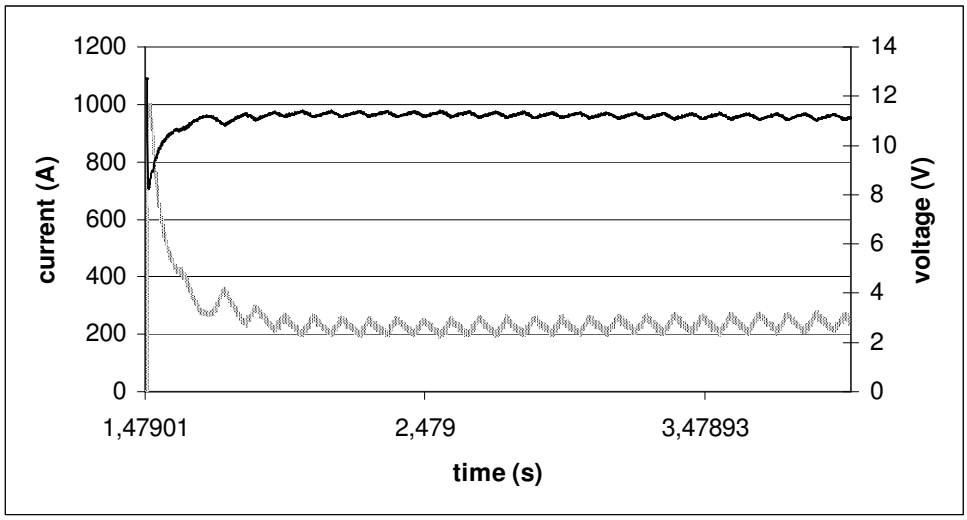

Diagram 6.3: Measured starter motor current and the voltage at 22°C.

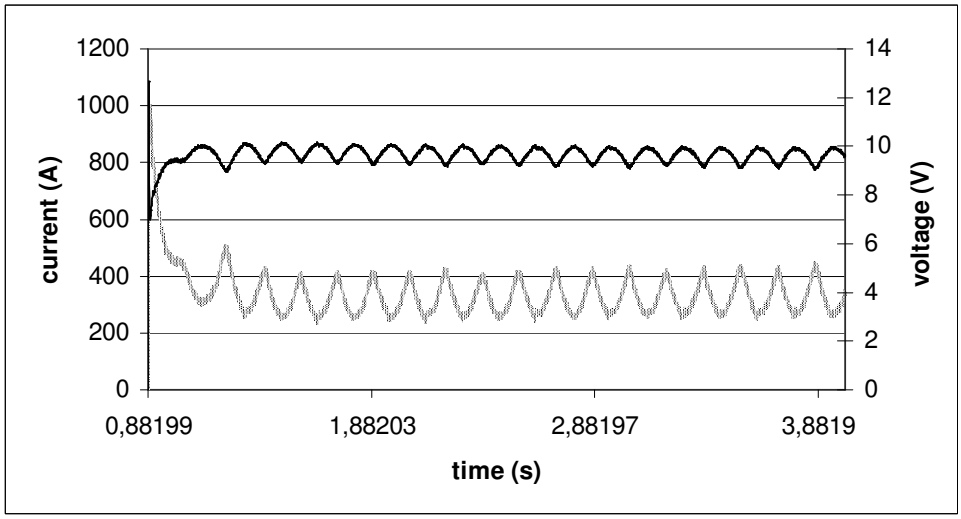

Diagram 6.4: Measured starter motor current and the voltage at -19°C.

Note that for the Diagrams 6.3 and 6.4 the grey curves are the starter currents and the black curves are the voltages.

The results for the rest of the temperatures can be found in Appendix x.

Chapter 7

Discussion

By comparing the simulated engine speed with the measured speed, you recognize some similarities and some differences as seen in Diagrams 5.1 and 5.2 for the simulations and Diagrams 6.1 and 6.2 for the measurements. The speed is quite lower in the simulation and there is less variations than in the measured. The differences in speed could be related to a too high mean friction in the engine model and possible reasons to the lower speed variations in the simulation could be that the engine friction model is not accurate enough in torque variations during the cycle. Another reason could be that the starter current and therefore the generated torque from the starter motor varies too much by the engine total torque variations. The reason for the high current variation could be the dramatic changes in Ke and Kt during the total torque variations, while it should change linearly as it is mentioned in the section 3.7.3. The differences between the measured and simulated currents are shown clearly by comparing the Diagrams 5.3 and 5.4 with 6.3 and 6.4.

The mean value of the speed is simulated better at -19°C compared with 22°C, but the speed variation is relatively higher in the simulation at the lower temperature. A reason for that could be that the engine model is not validated enough and that it needs more temperature dependency factors than the oil viscosity. The starter motor current at -19°C is higher than the one at 22°C in the simulation and that corresponds with the results from the measurement which means that the complete model follow the temperature variation approximately.

Recommendations for further work and improvement of the starter system model can be found for each part in the starter motor and the engine chapter respectively.

References

1. (http://www.synopsys.com/products/mixedsignal/saber/saber.html)

2(http://www.synopsys.com/products/mixedsignal/saber/mast_ds.html)

vv